Annals of Nuclear Energy 203 (2024) 110503

Contents lists available at ScienceDirect

Annals of Nuclear Energy

journal homepage: www.elsevier.com/locate/anucene

Evaluations of radionuclide activity releases into environment during loss of coolant accidents using the ASTEC code in pressurized water reactors within design basis and design extension conditions

Stefano Ederli [a,*], Patrick Drai [b], Dorel Obada [c], Nathalie Girault [b], Fulvio Mascari [d]

[a] ENEA - Casaccia, Via Anguillarese 301, 00123, Roma, Italy
[b] IRSN - Centre de Cadarache, B.P. 3, 13115 Saint-Paul-lez-Durance Cedex, France
[c] IRSN - 31 avenue de la Division Leclerc, 92260 Fontenay-aux-Roses, France
[d] ENEA - Bologna, Via Martiri di Monte Sole 4, Bologna, Italy

ARTICLE INFO

Keywords:
PWR
LOCA
DBA
DEC-A
ASTEC
R2CA

ABSTRACT

The work described in this paper was carried out within the R2CA (Reduction of Radiological Consequences of design basis and extension Accidents) project, funded in HORIZON 2020 and coordinated by IRSN (France). An increase of the level of Nuclear Power Plant (NPP) safety by consolidated and more realistic evaluations of the Radiological Consequences (RC) of Design Basis Accidents (DBA) and a strengthening of the assessments of the NPP safety levels by considering accidental situations more severe than those integrated in plant designs (i.e belonging to Design Extension Conditions domain) were the two main motivations behind this project.

More specifically, the project aims at consolidating and/or refining the assessments of the radiological consequences of explicit accidental scenarios within Design Basis Accidents (DBA) and Design Extension Conditions (DEC-A conditions without significant fuel degradation) in Light Water Reactors (LWR) through the improvements of existing code predictability; the upgrading of calculation chains and methodologies; the development/refinements of models. Within the Work Package 2 of the project, coordinated by TRACTEBEL and dedicated to calculation methodologies, existing methodologies or calculation chains and simulation tools have been applied to run a first batch of calculations dealing with different reactor types: PWR (Pressurized Water Reactor), BWR (Boiling Water Reactor), VVER (Water-Water Power Reactor) and EPR (European Pressurized Reactor). Loss Of Coolant (LOCA) and Steam Generator Tube Rupture (SGTR) accidents have been selected for the exercise and bounding scenarios of the DBA and DEC-A domains have been analysed. The results of this first set of calculations will be used as a reference to quantify the gains obtained by the updated methodologies/simulation tools developed within the project.

This paper describes the results of the first batch of calculations, performed with the ASTEC integral code, simulating LOCA scenarios (DBA and DEC-A categories) in a PWR 900 MWe with a focus on the predicted number of failed fuel rods and Source Term (ST) in the environment governing the RC. Limitations of the used approach are outlined, as well as the needs for further upgrading the calculation chains are proposed in the light of the improvement that was planned within the project in Work Package 3 (WP3: LOCA – Loss of Cooling Accidents), coordinated by IRSN and dedicated to the improvement of code models dealing with LOCA scenarios.

1. Introduction

After the Fukushima Daiichi Nuclear Power plant (FDNPP) accident, the Research and Development (R&D) on Severe Accidents (SAs) had a renewed interest covering different investigation fields such as the improvement of codes for SA sequence simulations and consequence evaluations or research programs dealing with Severe Accident Management (SAM). All these R&D efforts led to consolidated evaluations of Radiological Consequences (RC) and to improvements of SAM and mitigation strategies. When further integrated in PSA level 2 studies, the effective reduction of the risks associated to all main categories of SA

* Corresponding author.
E-mail addresses: stefano.ederli@enea.it (S. Ederli), patrick.drai@irsn.fr (P. Drai), dorel.obada@irsn.fr (D. Obada), nathalie.girault@irsn.fr (N. Girault), fulvio.mascari@enea.it (F. Mascari).

https://doi.org/10.1016/j.anucene.2024.110503
Received 26 July 2023; Received in revised form 19 March 2024; Accepted 25 March 2024
Available online 6 April 2024

Nomenclature

AFW	Auxiliary Feed Water
AI	Accumulators Injection
ASTEC	Accident Source Term Evaluation Code
ATF	Accident Tolerant Fuels
BAF	Bottom Active Fuel
BEPU	Best Estimate Plus Uncertainty
BWR	Boiling Water Reactor
CESAM	Code for European Severe Accident Management
CL	Cold Leg
CSS	Containment Spray System
DBA	Design Basis Accidents
DEC	Design Extension Conditions
DEC-A	Design Extension Conditions without significant fuel degradation
DEC-B	Design Extension Conditions with significant fuel melting
DG	Diesel Generator
ECCS	Emergency Core Cooling Systems
EOC	End Of Cycle
EPR	European Pressurized Reactor
EU	European Union
FA	Fuel Assembly
FDNP	Fukushima Daiichi Nuclear Power plant
FP	Fission Product
GRS	Gesellschaft für Anlagen- und Reaktorsicherheit
HL	Hot Leg
HPIS	High Pressure Injection System
IB	Intermediate Break
IRSN	Institut de Radioprotection et de Sûreté Nucléaire
IVMR	In Vessel Melt Retention
KIT	Karlsruher Institut für Technologie
LOCA	Loss Of Cooling Accident
LOOP	Loss Of Off-site Power
LPIS	Low Pressure Injection System
LWR	Light Water Reactor
MFW	Main Feed Water
NPP	Nuclear Power Plant
PCT	Peak Cladding Temperature
PWR	Pressurized Water Reactor
PZR	Pressurizer
RC	Radiological Consequences
RCS	Reactor cooling system
RWST	Refuelling Water Storage Tank
R2CA	Reduction of Radiological Consequences of design basis and extension Accidents
SGRV	Steam Generator Relief Valves
SGTR	Steam Generator Tube Rupture
SA	Severe Accident
SAM	Severe Accident Management
SCRAM	Safety Control Rod Axe Man
SG	Steam Generator
SB	Small Break
ST	Source Term
TAF	Top Active Fuel
VVER	Water-Water Power Reactor

conditions was also highlighted and therefore also the very conservative evaluations of risks usually done for accidents within the Design Basis Accident (DBA) domain.

They also confirmed that the evaluations of RC of accidents within the DBA domain usually are done with very conservative deterministic assumptions (EU, 2001; Regulatory Guide, 2003) mostly based on decoupled approaches which prevents for an explicit quantification of the gains, notably in terms of RC, of additional safety measures or devices. For example, for LOCA DBA source term evaluations, various methodologies, approaches and assumptions were currently used for existing reactors where assumptions on a fixed number of failed rods were often used (Report, 2016). As a consequence, most of the LOCA DBA RC were assessed with an assumed proportion of failed fuel rods ranging from 1 to 100 % and very few methodologies were really suited to evaluate more realistically the number of failed rods to the difficulties in predicting the clad ballooning and burst in LOCA DBA conditions (most of the criteria having being developed to predict flow blockage for reflooding evaluations) and in modelling a full core pin-by-pin due to computational-time consumption. Finally, an additional outcome of the reviews of safety analysis approaches, made in particular in Europe after FDNPP accident, was the importance to strengthen globally the assessment of the safety level of Nuclear Power Plants (NPPs) by considering additional accidental situations, Design Extension Conditions (DEC), more severe than those integrated during the design of the plants (i.e. additional events or combination of events) for which specific provisions have to be also designed. This is well pointed out by the definition of the DEC accidents category (International Atomic Energy Agency, 2016; International Atomic Energy Agency, 2021), further subdivided into DEC-A domain, addressing accidental scenarios for which the prevention of significant fuel degradation can be achieved and DEC-B domain, dealing with accidental transients characterized by significant fuel melting. Indeed, as part of the defence in depth (Defence in depth in nuclear safety, 1996), analysis of DEC (WENRA Safety Reference Level for Existing Reactors, 2021) shall be undertaken with the purpose of further improving the NPP safety by considering scenarios and/or conditions that will have to be withstood more challenging than those currently considered for the DBAs.

In this context, one of the objectives of Reduction of Radiological Consequences of design basis and design extension Accidents (R2CA) project is to propose upgraded methodologies and improved code models for the estimation of RC of accident scenarios of both DBA and DEC-A domains. For this purpose, the existing codes and methodologies have been tested, in the task 2.3 of the project, by running a first batch of reactor calculations regarding different reactor types: PWR, BWR, VVER and EPR.

The paper illustrates the work performed, with the Accident Source Term Evaluation Code (ASTEC) (Chailan, et al., 2017; Chatelard, 2016; The ASTEC Software Package, 2023), on Loss of Coolant Accident (LOCA) scenarios of both DBA and DEC-A domains in a generic PWR 900 MWe. The first section is dedicated to the description of simulated accidental scenarios. ASTEC code and developed plant model are detailed in the second section. The third and fourth sections provide the obtained results, respectively for DBA and DEC-A transients, which are discussed in the final section that reports the main conclusions of performed work.

The obtained results will be used as reference to demonstrate the improvements of models and calculation schemes, for the estimation of RC, achieved along the project. Such a demonstration is in progress, within the task 2.5 of the project, by running a second batch of reactor calculations taking advantage of these improvements among which, of particular interest for LOCA scenario RC evaluations, an improved evaluation of the number of failed fuel rods (Taurines, 2023).

The final objectives of the updated calculations of Source Term (ST) or RC of these DBA and DEC-A accidents is to demonstrate that the releases of radioactive products outside the NPP, following these transients, have limited consequences for public health and the environment. These studies then contribute to verify the validity of the safety provisions and measures taken respectively during the NPP design

and its operation, in particular with regard to the confinement of radioactive products.

2. Scenarios and main assumptions

Both one design basis and one design extension transients in a PWR 900 MWe were simulated within the R2CA project. These scenarios considered as bounding scenarios from the RC point of view were chosen from the safety report on RC issued at the time of the fourth decennial visit of the French PWR 900 MWe reactors (Level 2 Probabilistic Safety Assessment for French, 2008). R2CA project was restricted to DEC-A scenarios with no significant fuel melting.

For each scenario (DBA and DEC-A), two cases have been studied, characterized by some differences on initial/boundary conditions, accident management and assumptions that were independently defined by the ENEA and IRSN teams, in charge of ASTEC simulations within R2CA project, according to their own practices and experience.

The results of the two cases will be illustrated and discussed briefly. However, an in-depth comparison and analysis to characterize the effect of each user's option (initial/boundary conditions, assumptions, etc.) on code results, is beyond the scope of the article. Indeed, the purpose of R2CA project wasn't to do a benchmark exercise between different codes or users but to compare initial partner's calculations with final calculations, the latter performed after update of models, simulation tools and calculation chains.

Table 2.1 provides a synthetic view of considered scenarios (break size, localization), of the initial conditions before transients as well as of the main assumptions and hypotheses. A more detailed description is provided in the following sections of the paper.

Table 2.1
Scenarios, initial conditions and main assumptions considered in the calculations for DBA and DEC-A conditions.

			DBA		DEC-A	
			Case 1	Case 2	Case 1	Case 2
Initial and boundary conditions	Power	% of nominal Power at accident onset	100	100	1*	1*
		Axial distribution of FPs (decay-heat profile)	Flat	Flat	Flat	Flat
		Radial distribution of FPs (decay-heat profile) per modelled groups of fuel rods	1.13;1.18; 1.12;1.06; 0.78	1.10;1.20; 1.16;1.08:0.74	1.10;1.20; 1.16;1.08:0.74	1.13;1.18; 1.12;1.06; 0.78
	Burn-up and Fuel cycle	GWd/t 3rd cycle	30 EOC	30 EOC	30 EOC	30 EOC
	Gap inventory	% of core inventory	Cs (5.0); Xe, Kr (3.0); I (1.7); Te, Sb (0.01); Sr, Ba (0.0001)	Cs (5.0); Xe, Kr (3.0); I (1.7); Te, Sb (0.01); Sr, Ba (0.0001)	Cs (5.0); Xe, Kr (3.0); I (1.7); Te, Sb (0.01); Sr, Ba (0.0001)	Cs (5.0); Xe, Kr (3.0); I (1.7); Te, Sb (0.01); Sr, Ba (0.0001)
	RIP	bar	30	50	30	30
Accidental scenario	Initiator		IB 16.3′ in CL	IB 16.3′ in CL	SB 4′ in HL	SB 4′ in HL
	Additional failures		LOOP + ½ DG	LOOP + ½ DG	no	no
	Actions of safeguard & safety and delays		Automatic start of ECCS, AI & CSS, ECCS injection in CL	Automatic start of ECCS, AI & CSS, ECCS injection in CL	Manual start of ECCS after 33 min in CL	Manual start of ECCS after 36.5 min in CL
Fuel rods failure and Radiological Consequences calculation in the environment	Rupture criterion		EDGAR + 25 % max hoop strain	CHAPMAN + 25 % max hoop strain	EDGAR + 40 % max hoop strain	EDGAR + 40 % max hoop strain
	Duration of releases	h	48	48	48	48
	Paths of releases		AUX	DCL	DCL	AUX
	Routes included		1.2	1.2	1.2	1.2
	Considered doses		T, E, I	T, E, I	T, E, I	T, E, I

*Residual power after 2 h from 100% Nominal Power (NP).
RIP Rod Internal Pressure at room Temperature.
IB/SB Intermediate/Small Break.
CL/HL Cold/Hot Leg.
ECCS Emergency Core Cooling Systems.
LOOP Loss-Of-Offsite-Power.
DG Diesel Generator.
CSS Containment Spray System.
AI Accumulator Injection
DCL Direct containment leakages (non-filtered): 0,3% vol/day (at 4.85 bar).
AUX Leakages through auxiliary buildings.
1 Cloud exposure.
2 Inhalation
T Thyroid dose.
E Effective dose from external exposure.
I Effective dose from inhalation

2.1. Description of DBA scenario

The considered transient, part of the category 4 accident (International Nuclear and Radiological Event Scale (INES), 2023), is a 16.3 in. Intermediate Break (the largest IB considering the anti-deflection devices) occurring in one cold leg without pressurizer just upstream the primary pump. The Loss of Off-site Power (LOOP) is moreover assumed to occur at reactor shutdown together with the single failure of one over two emergency diesels leading to the loss of one over two trains of safety injection systems involving the Emergency Core Cooling Systems (ECCS) and Containment Spray System (CSS).

2.1.1. Initial and boundary conditions

The transient starts at nominal thermal power (approximately 2800 MW) and the fuel rods pressure at room temperature was assumed to be 30 bar or 50 bar, depending on the studied case (Table 2.1).

Regarding Fission Products (FPs), the assumed average FPs mass inventory at reactor shutdown corresponds to a core re-loading strategy of ¼ and to an End Of Cycle (EOC) fuel at equilibrium. FPs release from gap inventory was considered, no initial activity in the primary circuit was considered. This gap releases are assumed to be instantaneous once the fuel rod failure occurs. FPs gap inventory considered in the ASTEC input deck (Table 2.1) originates from the WASH-1400 (Ritzman, 1975) report and is valid for a UO_2 fuel with an average burn-up of 30 GWd/t and a reactor operating time of approximately 3 years.

Minor differences can be observed in Table 2.1 between studied cases, about radial factors which determine the FPs distribution (and decay-heat) in the 5 modelled groups of fuel rods (see next §3.2).

2.1.2. Safety systems and accident management

The automatic procedures set for French PWRs 900 MWe for managing the accidental sequence and the general rules used in Safety analyses were applied, in particular with regard to equipment and systems important for the reactor safety. The events and assumptions on safety systems availability and activation which characterize the simulated accident scenario are:

- Reactor scram on low pressurizer pressure (<131 bar).
- Turbine trip on scram actuation.
- Automatic start-up of available emergency diesel generator on Loss-of-off site Power (LOOP).
- Trip of primary pumps, stop of Main Feed Water (MFW) and pressurizer heaters because of LOOP.
- Start of ECCS on very low pressurizer pressure (<119.3 bar).
- Start of CSS on high containment pressure (>2.4 bar).
- Accumulator injection in primary loops for low primary pressure (P < 40 bar).
- Switch on recirculation mode of emergency systems (ECCS and CSS) for low level of Refuelling Water Storage Tank (<2.4 m).

2.2. Description of DEC-A scenario

The considered transient is a 4 in. Small Break (SB) occurring in one hot leg without pressurizer at primary vessel outlet at an intermediate subcritical hot state, two hours after the reactor shutdown (i.e. for reactor power approximately 1 % of its nominal power). This scenario is part of the complementary field of accidents studied in the safety analyses of French reactors. The additional provision is the ECCS manually activated by the operators.

2.2.1. Initial and boundary conditions

The transient starts two hours after the reactor shutdown when the reactor residual power is about 28 MW (i.e. 1 % of the nominal one (Table 2.1) and primary pressure and average temperature, lower than the nominal conditions, are respectively 70 bar (±2 bar) and 236 °C (±2.2 °C).

Regarding Fission Products, the same assumptions of DBA scenario have been considered (§2.1.1).

As already mentioned for DBA scenario, minor differences can be observed in Table 2.1 between studied cases, about radial factors which determine the FPs distribution (and decay-heat) in the 5 modelled groups of fuel rods.

2.2.2. Safety systems and accident management

The events and assumptions on safety systems availability and activation which characterize the simulated accident scenario are:

- Stop of main coolant pumps (MCPs) on low saturation criterion in primary circuit.
- Switch on recirculation mode of emergency systems (ECCS and CSS) for low level of Refuelling Water Storage Tank (<2.4 m).

For this scenario, in which an operator's intervention is required to start manually the ECCS, the considered delays are longer than 20 min. One must outline that sensitivity studies, performed on the time of ECCS activation by varying it within the range usually assumed in safety analysis studies (from 20 min up to 30 min), showed that no clad failure occurred and longer delays before the manual start-up of ECCS had to be considered. The two cases shown in this paper considered a delay of 33 and 36.5 min.

3. ASTEC code description and plant model

To estimate the FPs release to the containment atmosphere and further to the environment, the following data has been calculated by the code:

1. The failed fuel rod fraction and the corresponding FPs release to the primary system.
2. The release of FPs to the containment (in dry and wet phases).
3. The FP behaviour/retention in the containment.
4. The leaking rates from the containment and/or auxiliary buildings.

The main features of ASTEC code and the modelling of the PWR 900 MWe are reported in the sections below.

3.1. ASTEC code description

ASTEC (Accident Source Term Evaluation Code) is an integral code system developed by IRSN to compute SA scenarios, their entire phenomenology (steam explosion and containment mechanical integrity excepted) and their consequences in Water-Cooled Reactors (Chatelard, 2016), in particular Gen-II and Gen-III PWRs (The ASTEC Software Package, 2023). The code aims to simulate an entire SA sequence from the initiating event up to the releases of radioactive elements in the environment. It has a modular structure consisting of 13 coupled modules, each of these modules (Chailan, et al., 2017; Chatelard, 2016) simulating a reactor zone and/or a set of physical phenomena that can be used independently in a stand-alone mode, or all together in a coupled mode. The main modules and their functionalities are listed below:

- The two-phase thermal hydraulics of coolant flows in the reactor coolant primary and secondary systems including a 2D description of the reactor vessel (CESAR module).
- The degradation of materials within the vessel, when the temperatures reached under the effect of the core's residual power exceed a threshold leading to significant oxidization of the fuel rod claddings due to water vapor as well as various chemical interactions between the materials that make up either the fuel rods or the control rods (ICARE module).

- The release of FPs, particularly iodine, from any fuel material in the core, i.e. release from both standing pellets or relocated fuel compounds (either particulate debris or corium) (ELSA module).
- The transport of FPs as well as their physical and chemical behaviour in the cooling systems and in the containment where a detailed modelling of the aerosol behaviour (agglomeration, sedimentation, deposition on structures by diffusion or thermophoresis) the iodine chemistry and the physico-chemical behaviour of different iodine species (molecular iodine, gaseous organic iodides, iodine oxides aerosols…) in the containment vessel is included (SOPHAEROS module).
- The thermal-hydraulics within the containment using a 0D volumes approach, classically called "lumped-parameter code" (CPA module).

Furthermore, ASTEC evaluates the radioactivity of the isotopes and the associated residual power in all parts of the reactor, as well as dose rates in the containment (ISODOP and DOSE modules).

Several linkages to other tools are also available which can be used for processing the input and output of the code simulations or for uncertainty and sensitivity analyses.

Presented calculations have been performed with the ASTEC V2.2 version, released in April 2021.

3.2. ASTEC modelling of PWR 900 reactor

The used ASTEC modelling and input decks of the PWR 900 MWe are issued from previous work, performed for example within the past EU-CESAM project (Chatelard, 2017; Nowack et al., 2018) and for PSA level 2 studies (Raimond, 2013).

Fig. 3.1 and Fig. 3.2 respectively provide a schematic view of ASTEC model and nodalization for the reactor vessel and the Reactor Coolant System (RCS), the latter consisting of three independent primary and secondary loops.

The core, composed of 157 Fuel Assemblies (FAs) is modelled, by considering 5 groups of rods contained into 5 radial fluid channels. The number of FAs represented by each group of rods is reported in Fig. 3.1 right. The average FPs mass inventory determining the decay heat, automatically computed by ISODOP module of ASTEC, is radially distributed in the 5 groups of rods by using user-selected weighting factors in the dataset. Slightly different values of radial weighting factors have been considered, depending on studied case, as mentioned before and reported in Table 2.1.

One must point out that, assuming one representative fuel rod per channel in the core, all the fuel rods of a same group will fail at the same time and location. This is a strong approximation as the fuel assembly behaviour in a channel will probably be different and dependant on their in-reactor life (different irradiation history and various location occupied in the core during the reactor cycles).

Nodalization of RCS primary and secondary side is illustrated by Fig. 3.2.

The containment modelling (Fig. 3.3) considers 13 volumes for the main containment zones (dome, reactor cavity, sump, etc). External buildings (i.e. auxiliary building (BAN), fuel building (BK), outlying building (BW) and unventilated buildings (BNV)) are modelled or not, depending on studied case. Leak paths to the environment in case of auxiliary building consideration (i.e. directly from containment and through external buildings) are indicated in the Fig. 3.3. More details about leakages simulation are given in §3.3.2.

3.3. Main ASTEC modelling options considered

The main modelling options considered for simulated the DBA and DEC-A scenarios are described below.

3.3.1. Cladding burst

Several model/criteria can be selected in ASTEC code to predict the cladding burst:

- EDGAR burst criterion, based on true burst hoop stress function of cladding temperature (Topin et al., 2021; Coindreau, 2020; Pettersson, 2009).
- CHAPMAN burst criterion, based on a temperature condition function of engineering hoop stress and temperature derivative (Chapman, 1979).
- A user dependent criterion (EPMX parameter), defining the maximum allowed cladding hoop strain before failure (default value in the code 40 %) (Topin et al., 2021).
- NUREG-630 criterion, based on a hoop strain condition function of cladding temperature (Powers and Meyer, 1980), is also contemplated by the code but it has been disabled after finding unphysical results in some of performed simulations.

It should be noted that only EDGAR and CHAPMAN are alternative concurrent burst criteria. EPMX parameter or NUREG-630 criterion are additional criteria, used in combination with EDGAR or CHAPMAN ones, the first criterion with is fulfilled leading to the cladding burst.

Used options, depending on analysed scenario and considered case are reported in Table 2.1 and they will be recalled in the description of performed simulations.

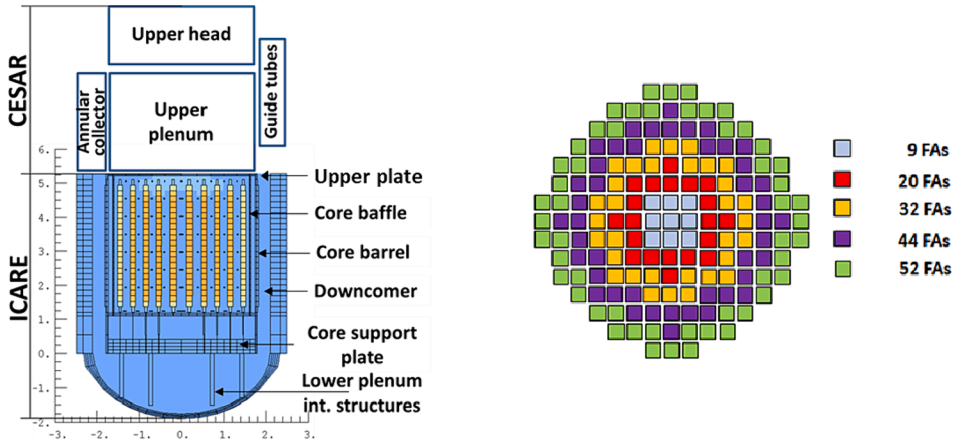

Fig. 3.1. ASTEC code vessel and core modelling.

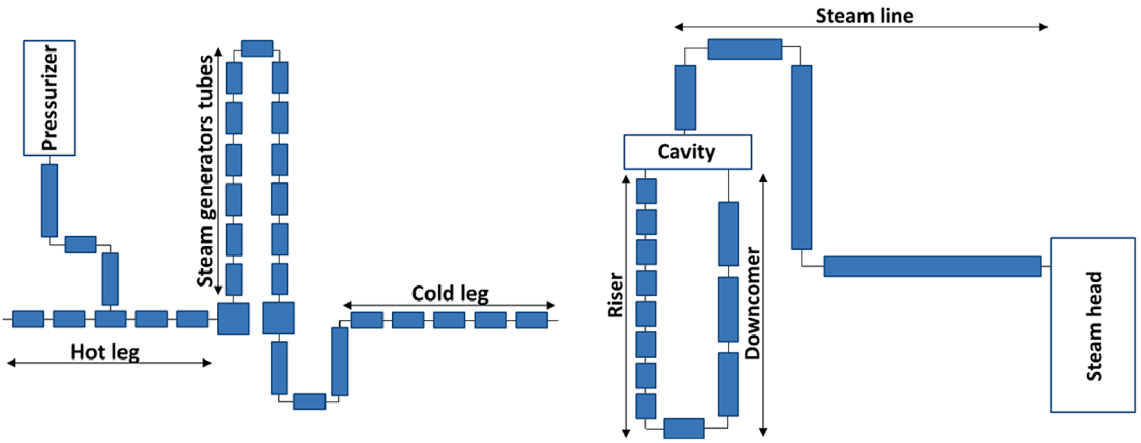

Fig. 3.2. ASTEC code modelling of primary (left) and secondary (right) RCS.

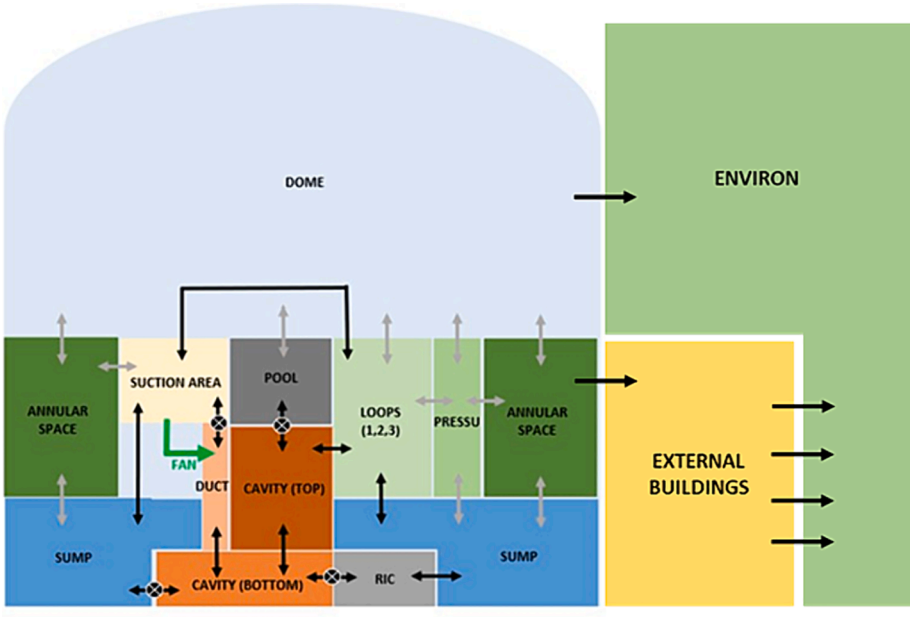

Fig. 3.3. Containment nodalization.

3.3.2. Containment leakages

Leakage flows are modelled, with simple equations defined by users, as a function of the computed pressure difference between containment and surrounding areas, i.e. environment and neighbouring external buildings if the latter are modelled. Both options (with and without external buildings) were considered depending on the simulated case (Table 2.1).

In the case of external building simulations, the user's equations were defined to have, for a given pressure difference, a fixed distribution of containment leaks between the environment and the external buildings; the 14 % of the total leak flow going from the containment dome to the environment (Fig. 3.3) and the 86 % from the outer side of the containment (annular space in Fig. 3.3) to the four simulated external buildings (i.e. 39 % to outlying building, 9 % to unventilated buildings and 19 % respectively to auxiliary and fuel buildings). The leakage through the external buildings is then released without filtration to the environment, because of natural air circulation (filtered venting systems are considered unavailable). The presence of external buildings therefore contributes to reduce (through wall deposition) and delay the release of FPs in the environment.

In the case without external buildings, the 100 % of leakage flow was directly released into the environment without considering any filtration system of FPs within the containment and without the mitigation of FPs release, operated by the external buildings.

The containment leakage is the only phenomenon modelled to account for the FPs release in the environment.

4. DBA transient analyses

Before running the transient, to obtain the steady-state operating reactor parameters, a first calculation was performed with the appropriated regulations and allowing to check the main thermohydraulic values in the core, primary loops and steam generators (primary pressure, core inlet/outlet temperatures, mass flow rates in the primary loops, pressures in steam-generators…).

The main features and differences of the two studied cases are given in Table 2.1 and briefly recalled hereafter.

Case 1

- Burst criterion: EDGAR combined with EPMX (maximum cladding hoop strain) = 25 % (default value = 40 %).
- Fuel rods pressure at room temperature = 30 bar.

– External buildings are simulated.

Case 2

– Burst criterion: CHAPMAN combined with EPMX (maximum cladding hoop strain) = 25 % (default value = 40 %).
– Fuel rods pressure at room temperature = 50 bar (mean equivalent pressure increase to account for the diversity of fuel rod internal pressures as a function of differences in the irradiation history of PWR900 core assemblies coexisting within the same concentric ring).
– External buildings are not simulated. Direct leaks from containment building to the environment are considered.

Results presented in the following sections are in general based on Case 1 simulation. Differences with Case 2 are outlined only if relevant for the discussion of results. In the absence of indication, presented results refer to Case 1.

4.1. *Thermal-hydraulic and mechanical behaviour*

The calculated transient scenario proceeds in the four well-known successive phases:

- The blow-down phase: at the beginning of the accident a significant flow of subcooled water escapes from the break (Fig. 4.2) leading to a fast decrease of primary pressure (Fig. 4.1) and water inventory in the primary loops and vessel. The progression of core uncovering can be observed in Fig. 4.3 which shows the evolution vs. time of water collapsed level in the 5 radial fluid channels of reactor core, level 0 corresponding to the Bottom Active Fuel (BAF).

After approximately 10 s from the start of transient, the primary pressure is low enough to reach saturation in the primary loops and both liquid and steam come out of the break (Fig. 4.2) slowing down the primary pressure decrease (Fig. 4.1). Shortly after, dry-out conditions arise at the top of the core leading to the sudden increase of fuel rod claddings temperatures that can be observed in Fig. 4.8, displaying the evolution vs. time of the maximum cladding temperature for the 5 groups of fuel rods. The computed cladding heat-up is very fast. Indeed, the reactor SCRAM occurred at about 6 s from the transient beginning, few seconds before the dry-out onset, when the fuel was yet at very high temperature (above 1500 K in the four innermost groups of fuel rods, as illustrated by Fig. 4.9) that implies a strong heat release to the cladding. The heat-up of fuel rod claddings is stopped (reaching a peak just above 1000 K in the 2nd and hottest group of fuel rods) by a temporary reestablishment of core cooling, due to cold water coming into the vessel from intact loops. After a rather temporary increase, due to the mentioned ingress of water in the vessel, the collapsed water level continues to drop and, at about 28 s, when the core is practically totally uncovered (Fig. 4.3), the heating of fuel rods starts again (Fig. 4.8).

On the containment side, the water-steam flow discharged from the break leads to the immediate increase of both temperature and pressure in the containment (Fig. 4.4 and Fig. 4.5). Then both containment gas temperature in the dome and the containment pressure decrease, following CSS automatic triggering on pressure criteria.

- The refill phase: the vessel refilling begins at about 50 s, when the water collapsed level is about 1 m below the BAF (Fig. 4.3) and

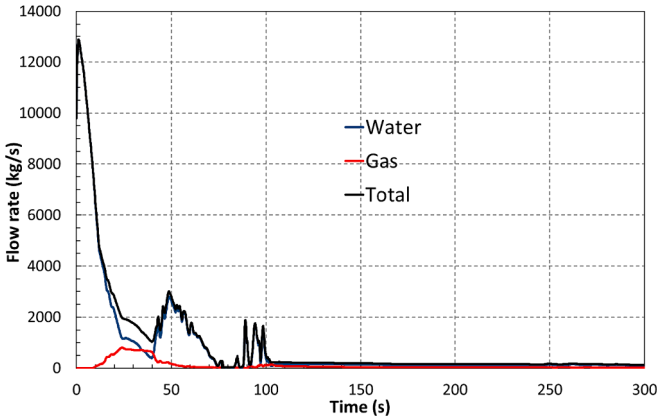

Fig. 4.2. Break mass flow rate (DBA).

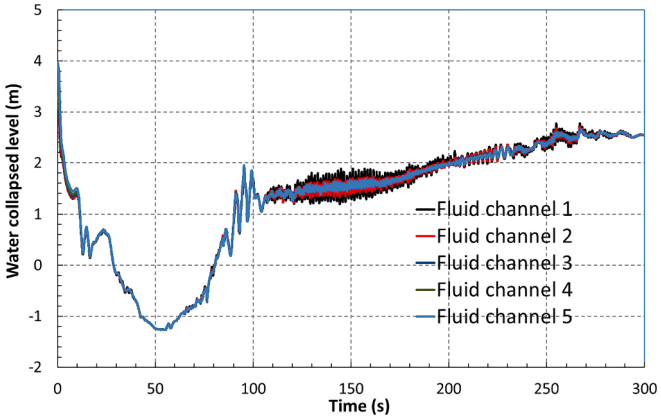

Fig. 4.3. Collapsed water level in the core (5 fluid channels) from BAF (DBA).

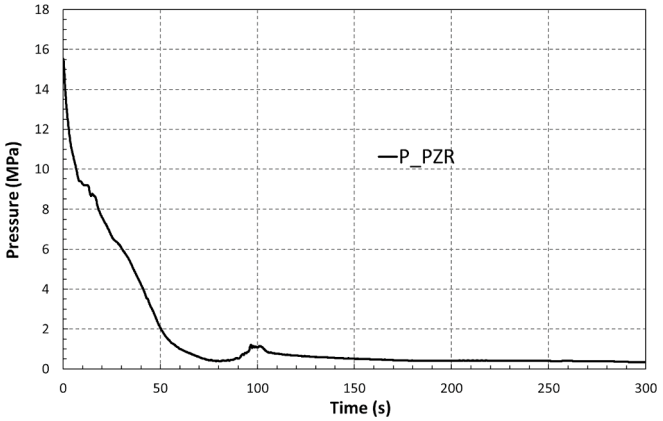

Fig. 4.1. Primary pressure evolution (DBA).

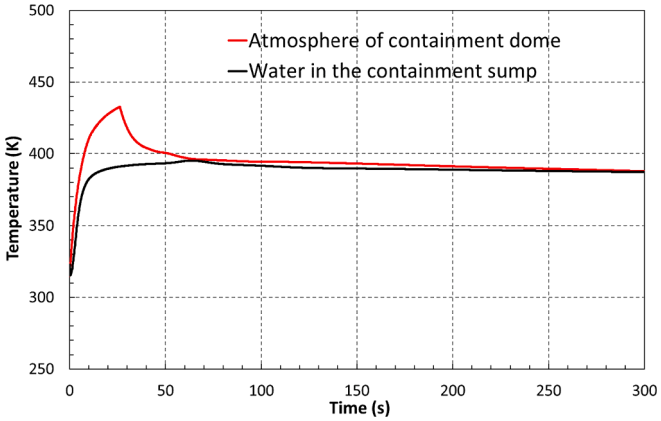

Fig. 4.4. Containment temperature in the short term (DBA).

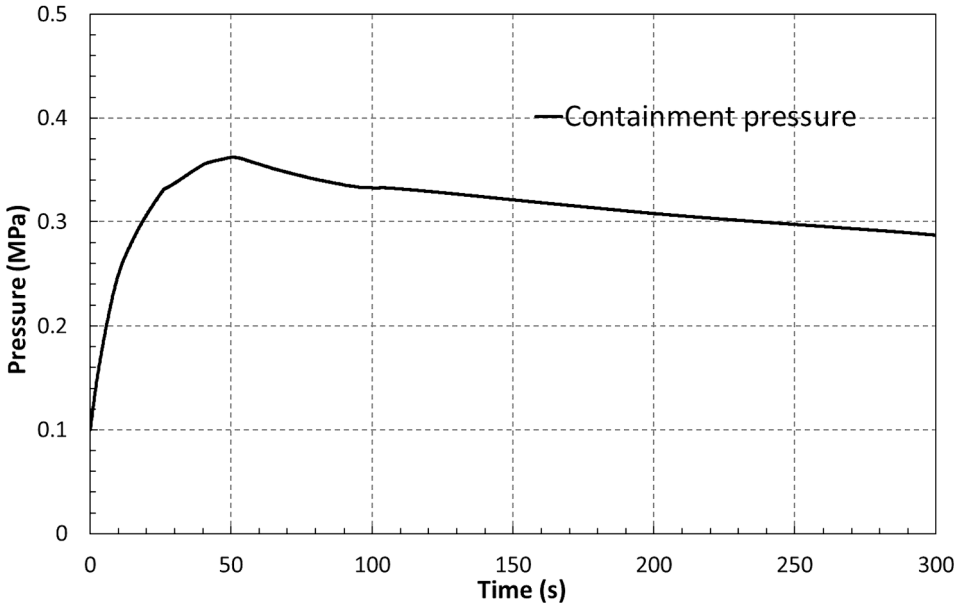

Fig. 4.5. Containment pressure in the short term (DBA).

several seconds after the start of ECCS water injection (36.1 s) and the onset of accumulators discharge (39.6 s). This is because, in a first time, the injected water is almost completely lost through the break.

- The core reflood phase: the water collapsed level increases progressively and it reaches the BAF after about 80 s of transient (Fig. 4.3) allowing the reestablishment of two-phase flow in the core and starting the cooling phase until complete quenching of all fuel rod groups, that takes place after about 160 s of transient (Fig. 4.8).
- The last phase is the long-term cooling phase: the reestablishment of water inventory in the reactor primary system progresses slowly, due to the quite large break and the loss of one over two safety injection systems. At the end of simulated transient (50 h), only cold legs and vessel downcomer are completely refilled. The collapsed water level in the core is at about 1 m below the hot legs inlet and, therefore, the upper plenum of the vessel, hot legs and SGs primary side (water box and U-tubes) remain empties. Regarding the containment, its behaviour is characterized by small variations of temperature and pressure, occurred when ECCS and CSS switch in recirculation mode (both safety systems switch from RWST to containment sump with higher water temperature) (Fig. 4.6 and Fig. 4.7).

The mechanical behaviour of the 5 groups of fuel rods is coupled with their temperature evolution (Fig. 4.8) that drives both internal fuel rods pressure and cladding deformation by creep. Fig. 4.10 shows, for each of the 5 groups of fuel rods, the computed difference between their internal pressure and the pressure of surrounding coolant. Both Case 1

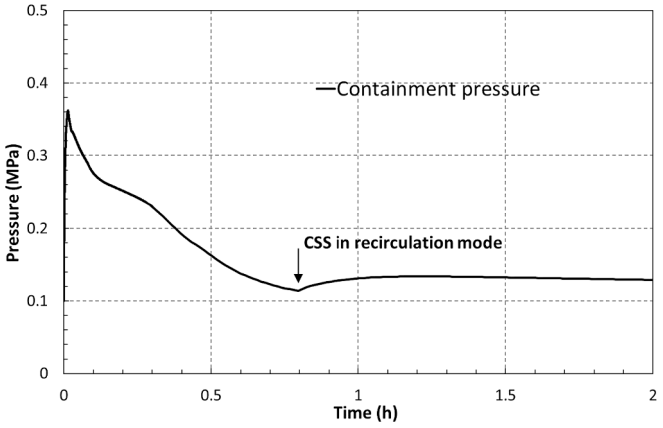

Fig. 4.7. Containment pressure in the long term (DBA).

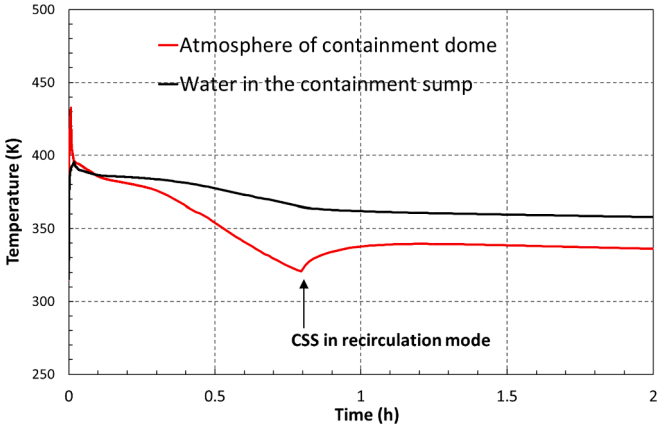

Fig. 4.6. Containment temperature in the long term (DBA).

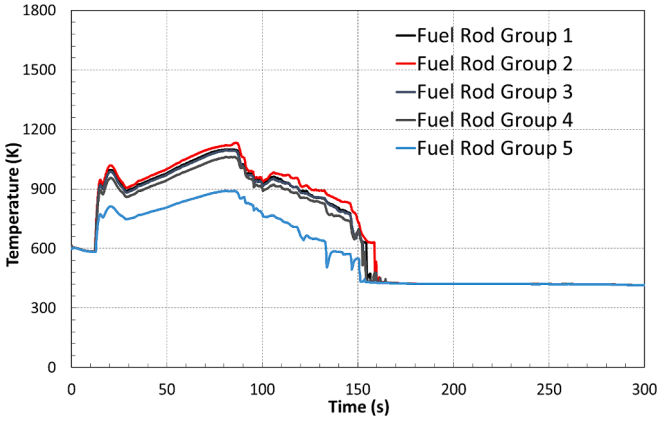

Fig. 4.8. Maximum cladding temperature (PCT) in the 5 groups of fuel rods (DBA).

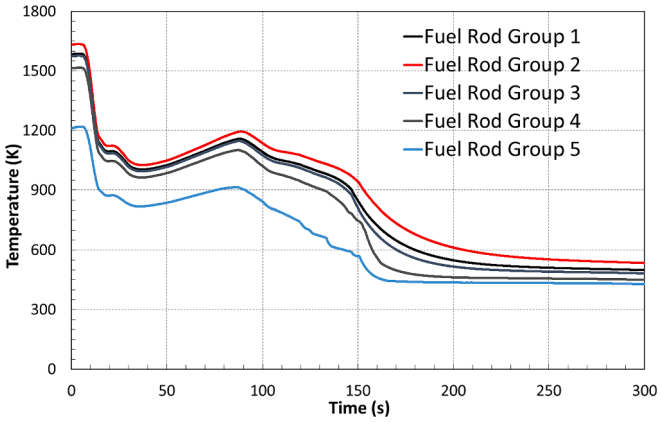

Fig. 4.9. Maximum fuel temperature in the 5 groups of fuel rods (DBA).

(Fig. 4.10 left) and Case 2 (Fig. 4.10 right) results are presented and, in agreement with the different pressure imposed at room temperature (30 bar and 50 bar respectively in Case 1 and Case 2), the computed pressure difference during the transient is quite lower in the Case 1.

The cladding burst, leading to the instantaneous depressurization of the fuel rods, can be easily identified in the curves of Fig. 4.10 by the pressure difference which instantaneously drops to 0. The failure is then observed in the 2nd group of fuel rods, representing 5280 fuel rods (12.7 % of the fuel rods in the core) in the Case 1 whereas the rods failure occurs earlier and involves the 2nd and 3rd group of rods for a total of 13,728 failed fuel rods, corresponding to the 33.1 % of the fuel rods in the core, in the Case 2.

Table 4.1 reports the number of failed fuel rods for each involved group with other data regarding the failure time and elevation as well as the burst criterion triggering the failure.

In Case 1, the cladding failure of the 2nd group of rods is not due to the fulfilment of the EDGAR burst criterion but it occurs when the hoop strain exceeds the set value of EPMX parameter (25 %). One must outline that cladding failure is not more observed in an additional simulation with EPMX = 40 % (default value). In such a case, the cladding hoop strain remains below 40 % and EDGAR criterion continues to be unattained.

In Case 2, the failure of both groups of fuel rods is whereas triggered by CHAPMAN criterion, based on cladding temperature and engineering stress, which is fulfilled when the hoop strain is much lower than the maximum hoop strain (25 %) set in the input-deck.

One must point-out that the fulfilment of CHAPMAN criterion is favoured by the higher fuel rods internal pressure assumed in Case 2, that complicates the comparison with Case 1. To assess in a rigorous way the impact of selected burst criterion on the prediction of the number of failed rods it was then decided to perform a series of sensitivity calculations using EDGAR and CHAPMAN criteria under the same conditions of fuel rods internal pressure and axial and radial power distribution. Obtained results showed that a higher number of failed fuel rods is always predicted by assuming CHAPMAN criterion which confirms to be more conservative than EDGAR one. Performed simulations also demonstrate that with EDGAR criterion the cladding failure can be predicted only in case of the most pessimistic initial conditions (i.e. by combining an increase of the fuel rod internal pressure at room temperature to a more pitted axial and radial power distribution profile).

From the results obtained, emerges forcefully that the modelling of cladding burst is of great importance, as well as a more refined modelling of the core, for a reliable estimation of the failed number of fuel rods in the simulated DBA LOCA scenario. Indeed, the cladding burst is a complex phenomenon, strongly influenced by several parameters among which the fuel rod initial state (i.e. power, irradiation history burn-up) is an important one.

That is why, within the R2CA project, great efforts were deployed to (Taurines, 2023; Taurines et al):

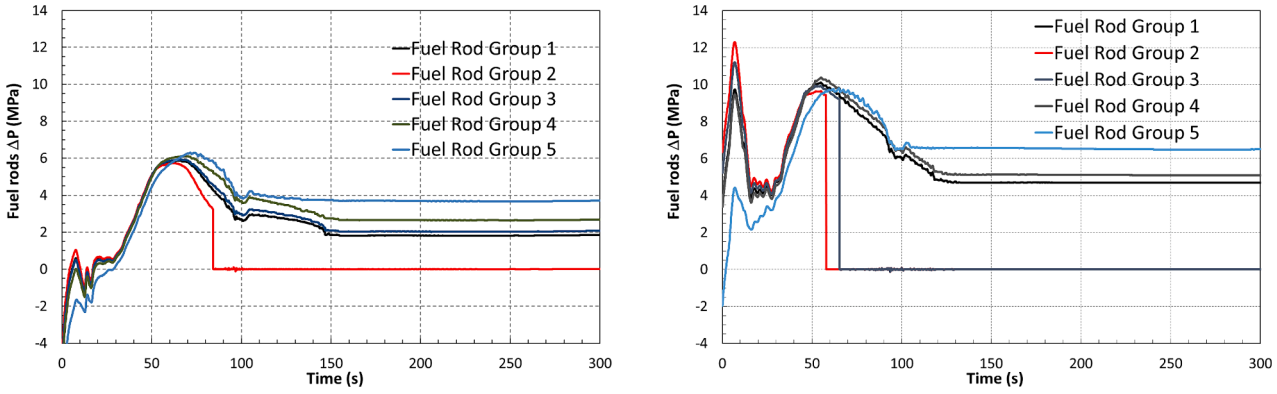

Fig. 4.10. Difference between the fuel rods internal pressure and the surrounding coolant in the 5 groups of fuel rods (DBA): Case 1 (left) and Case 2 (right) calculations.

Table 4.1
Characterization of cladding failures (DBA).

	Number of failed fuel rods		Failure time and (elevation from BAF)		Burst criterion triggering claddings failure	
	Case 1	Case2	Case 1	Case2	Case 1	Case2
Fuel rods 1	–	–	–	–	–	–
Fuel rods 2	5280	5280	84.13 s (~3 m)	57.83 s (~3 m)	Max. hoop strain = 25 %	CHAPMAN
Fuel rods 3	–	8448	–	65.10 s (~3 m)	–	CHAPMAN
Fuel rods 4	–	–	-	–	–	–
Fuel rods 5	–	–	–	–	–	–
Total (fraction)	5280 (12.7 %)	13,728 (33.1 %)				

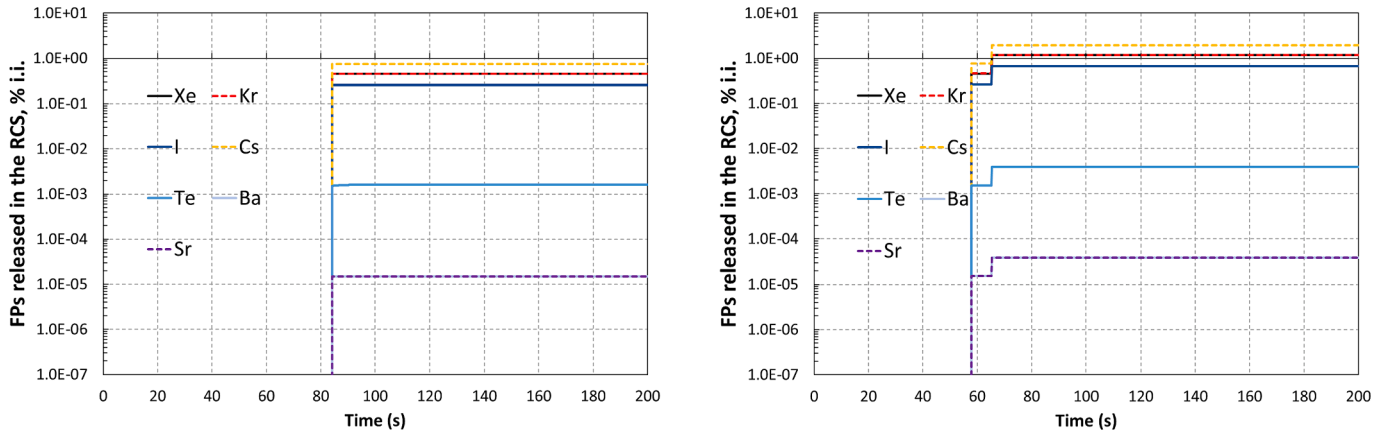

Fig. 4.11. FPs release from the core to the primary circuit (DBA): Case 1 (left) and Case 2 (right) calculations.

Table 4.2
FPs release to the primary circuit and the containment building after 50 h (DBA).

Element	Release to RCS (% i.i.)		Retention in RCS (% of released FPs)		Release to the containment (% i.i.)	
	Case 1	Case 2	Case 1	Case 2	Case 1	Case 2
Xe	4.5E-01	1.2E+00	0.0E+00	0.0E+00	4.5E-01	1.2E+00
Kr	4.5E-01	1.2E+00	0.0E+00	0.0E+00	4.5E-01	1.2E+00
I	2.6E-01	6.6E-01	7.8E+01	3.6E+01	5.7E-02	4.2E-01
Cs	7.5E-01	2.0E+00	8.0E+01	3.6E+01	1.5E-01	1.2E+00
Te	1.6E-03	3.9E-03	7.8E+01	3.8E+01	3.6E-04	2.5E-03
Ba	1.5E-05	3.9E-05	7.7E+01	3.6E+01	3.4E-06	2.5E-05
Sr	1.5E-05	3.9E-05	7.7E+01	3.6E+01	3.4E-06	2.5E-05

- Reassess the experimental data base and propose new criteria for the simulation of fuel rods cladding failure.
- Refine the core modelling to better discriminate the fuel assembly behaviour and evaluate the respective potential for burst of each fuel rod.

Some of proposed burst criteria have been therefore implemented in ASTEC code and they are applied in the 2nd run of reactor calculations to perform sensitivity studies and characterize the effect of burst criteria uncertainties on the estimation of failed rods number.

4.2. FPs behaviour from fuel to environment releases

In DBA LOCA scenario with no fuel degradation and rather low fuel temperatures (Fig. 4.9 shows that the maximum averaged fuel temperature, reached after the cladding burst in the 2nd group of fuel rods, is about 1200 K), the ST is mainly due to the release of FPs gap inventory.

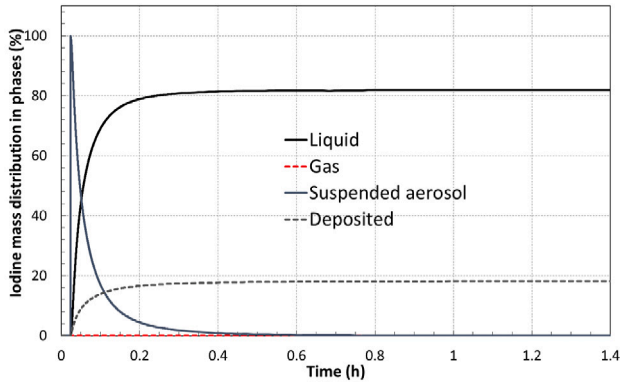

Fig. 4.12. Iodine mass distribution between different phases in the containment (DBA).

The release of FPs for the reactor core to the primary loops is illustrated by Fig. 4.11. Once the fuel cladding rupture occurs, the gap inventory is instantaneously released into the primary coolant circuits and a two steps release can be observed in Case 2, characterized by the failure of 2 groups of fuel rods (Fig. 4.11 right).

Table 4.2 presents the release to the primary circuits and to the containment building of some selected elements (Xe, Kr, I, Cs, Te, Ba and Sr), computed by Case 1 and Case 2. Except for the noble gases (Xe, Kr), the release to the containment in both studied cases is lower than the release from fuel rods, due to partial retention in the RCS mostly by aerosol deposition. Nonetheless, the Case 1 presents a more significant retention of FPs in the primary circuit, compared to Case 2 (Table 4.2). It is thought that the different timing of release contributes, at least in part, to the observed discrepancy. Indeed, the release in Case 1 occurs after 84.1 s from the initiating event when the steam flow rate, transporting the FPs to the break, is lower than at 57.8 s when the first release occurs in Case 2. A lower steam flow rate would facilitate the retention of FPs on the wall of the primary circuit, particularly in particulate form, giving a rationale for the observed behaviour.

Apart from the noble gases, the iodine is very important for the ST analyses due to its radiological impact and since it can form volatile species in the containment (I2, CH3I…). Fig. 4.12 presents the calculated iodine distribution between different phases in the containment. As for all the FPs aerosols, the suspended iodine as aerosol mass released from the RCS to the containment quite rapidly decrease due to aerosol deposition mostly by gravitational settling and to a less extent by deposition on the containment walls (diffusiophoresis, thermophoresis). Iodine is thus mostly and quickly dissolved into the containment liquid phase. The fraction of iodine in the containment gas phase is much lower.

Regarding the iodine speciation in the liquid phase, the most abundant species is the iodide ion I^- (Fig. 4.13 left), which is formed as a result of the dissociation of CsI and Cs_2I_2 that have settled from the suspended aerosols phase (Fig. 4.13 right). Since CsI and Cs_2I_2 are the

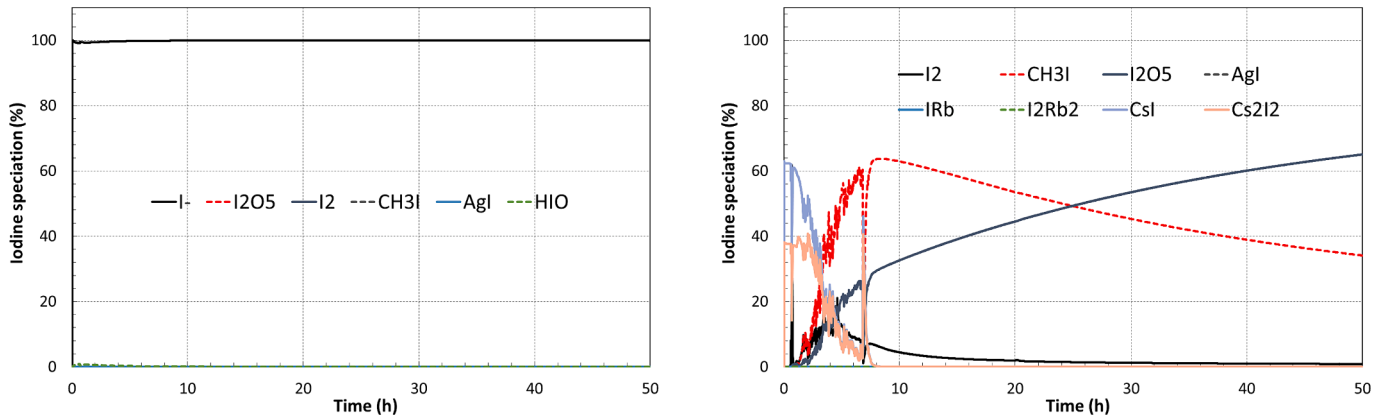

Fig. 4.13. Iodine speciation in the sumps (left) and the atmosphere (gaseous and suspended aerosols species) (right) in the containment (DBA).

Table 4.3
Cumulated activity (Bq) released in the environment, all leakage paths, by various isotopes after 50 h (DBA).

Isotope	Radioactive period	Release to the environment (Bq)	
		Case 1	Case 2
Xe133	5.2 days	4.8E+12	2.2E+13
Xe133m	2.2 days	1.2E+11	3.7E+11
Xe135	9.1 h	7.2E+11	5.3E+12
Xe135m	15.6 min	4.0E+10	7.2E+11
Kr85m	4.5 h	8.8E+10	8.4E+11
Kr88	2.8 h	1.4E+11	1.7E+12
I131	8 days	3.4E+09	5.8E+10
I132	2.2 h	1.6E+09	8.0E+10
I133	21 h	5.2E+09	1.2E+11
I135	6.6 h	3.4E+09	1.1E+11
Cs134	2.1 years	1.4E+09	2.4E+10
Cs136	13 days	4.6E+08	9.2E+09
Cs137	30 years	9.5E+08	1.6E+10
Te131m	30 h	2.6E+06	6.4E+07
Te132	3.2 days	2.8E+07	4.8E+08
Ba137m	2.5 min	8.1E+08	8.6E+09
Ba140	12.7 days	7.3E+05	1.3E+07
Sr89	50.6 days	8.0E+05	3.4E+06
Sr90	28.9 years	1.5E+04	1.9E+05
Sr91	9.6 h	1.5E+05	3.7E+06

major species in the suspended aerosols phase, they also constitute the major species in the deposited phase. In the long term, the most abundant iodine species in the containment atmosphere are the iodine oxides aerosols (commonly labelled I2O5 in the ASTEC code) and the organic iodine CH_3I. The latter is formed mainly by the interaction of gaseous I_2 with organic impurities present in the atmosphere and under the effect of radiation, whereas the former can be formed from both gaseous I_2 and CH_3I in presence of radiation. However, in absolute values their amount is insignificant since most aerosols have already settled down and the amount of available gaseous I_2 was never too high enough (see Fig. 4.12).

Table 4.3 presents the released activity in the environment for several selected isotopes, 50 h after the initiating event. For both cases the noble gases (Xe, Kr) contribute the most to the released activity (1–2 orders of magnitude greater than the next most released FPs), followed by iodine and caesium. In Case 2 (the most conservative), the calculated released activities are much higher for all isotopes compared to Case 1 due to higher number of failed fuel rods, lesser retention in RCS and also different assumptions regarding the containment leaks (direct containment leaks to environment vs. indirect and delayed containment leaks to environment through auxiliary buildings).

A more comprehensive analysis to discriminate the effect on ST estimation of user's choices, i.e. burst criterion, modelling approach for containment leakage, initial and boundary conditions, would have required much more time and effort and as mentioned before, it was beyond the project objectives and out of the paper purpose. Nevertheless, the identification of the more relevant uncertainty sources and the most impactful parameters affecting the ST estimation, is an important objective for better evaluating the RC and the safety margins in line with more sophisticated methods based on the Best Estimate Plus Uncertainty (BEPU) approach.

The RC at the outside of NPP have been estimated by a simplified model developed in R2CA (Bradt, 2021) that takes into account the event effective dose (due to external exposure when immersed in the cloud and inhalation) and the equivalent thyroid dose and consider six different classes of ages, Pasquill stability classes A and F with 1 m/s wind speed at 10 m altitude, and C and F with 2 m/s wind speed are considered for respectively short duration ($t \leq 6$ h) and longer duration ($t > 6$ h) releases. Each time the maximum dispersion coefficient value from these stability classes is retained for the radiological consequence evaluations. Table 4.4 reports, for adults, the thyroid equivalent dose and the total effective dose, by distinguishing external exposition and inhalation, at 1 km from emission point assumed at 60 m height, 2 days from the accident onset.

As expected, considered the rather low fuel temperatures reached during the transient and the associated very limited release of FPs, the computed doses are very low in both performed simulations. Higher values are observed in Case 2, in agreement with the greater activity released to the environment.

5. DEC-A transient analyses

As for DBA calculations, to obtain the steady-state operating reactor parameters, a first calculation was performed with the appropriated regulations and allowing to check the main thermohydraulic values in

Table 4.4
Computed dose (adults) at 1 km from emission point 2 days from accident onset (DBA).

	Thyroid equivalent dose (mSv)	Effective dose (mSv)		
		External exposition	Inhalation	Total
Case 1	0.002	0.0002	0.0002	0.0005
Case 2	0.066	0.0043	0.0092	0.0135

the core, primary loops and steam generators (primary pressure, core inlet/outlet temperatures, mass flow rates in the primary loops, pressures in steam-generators…).

In the chosen DEC-A scenario, the transient, a 4-inch break on one hot leg without PZR, is initiated 2 h after the reactor shutdown i.e. from an intermediate subcritical hot state characterized by a residual power corresponding to approximately 1 % of the nominal power (Table 2.1), a primary pressure of roughly 70 bar and a primary average temperatures of about 236 °C (509 K). The simulation of the accidental transient begins after a further ASTEC calculation starting from steady state at nominal power and aimed at reaching, with specially conceived regulations, such targeted initial conditions, including the residual power which is computed by the ISODOP module of ASTEC by considering the FPs inventory at reactor shutdown and the radioactive decay after 2 h of transient.

The main features and differences of the two studied cases are given in Table 2.1 and recalled hereafter.

Case 1

- Burst criterion: EDGAR combined with EPMX (maximum cladding hoop strain) = 40 % (default value).
- Fuel rods pressure at room temperature = 30 bars.
- External buildings not modelled. Direct leaks from containment building to the environment are considered.
- ECCS manual actuation after 33 min.

Case 2

- Burst criterion: EDGAR combined with EPMX (maximum cladding hoop strain) = 40 % (default value).
- Fuel rods pressure at room temperature = 30 bars.
- External buildings are simulated.
- ECCS manual actuation after 36.5 min.

Results presented in the following sections are mainly based on Case 1 simulation, characterized by earlier activation of ECCS and the absence of external buildings. Differences with Case 2 are outlined when they are relevant for the discussion of results. In the absence of indication, presented results refer to Case 1.

5.1. *Thermal-hydraulic and mechanical behaviour*

The transient scenario proceeds in several successive phases but with a slower kinetics than DBA.

After the fast initial depressurization (sub-cooled water flow at the break) and the temporary stabilization at a slightly higher value than the secondary side pressure, the primary pressure continues to decrease slowly (Fig. 5.1), until the ECCS activation at 33 min (Fig. 5.3), or 36.5 min in Case 2, leading to boiling in the core, primary pressure increase and to short-term water collapsed level oscillations (Fig. 5.4). Refilling and reflood start after 35 min (about 39 min in Case 2 characterized by delayed ECCS activation), when the water collapsed level is just below the BAF. After about 70 min (74 min in Case 2), the core is covered again and only water escapes from the break (Fig. 5.2).

From the beginning of the transient, until 60 – 70 min, the water-steam flow discharged from the break (Fig. 5.2) leads to an increase of both temperature and pressure in the containment (Fig. 5.5 and Fig. 5.6). However, given the fact that the break in the DEC-A scenario

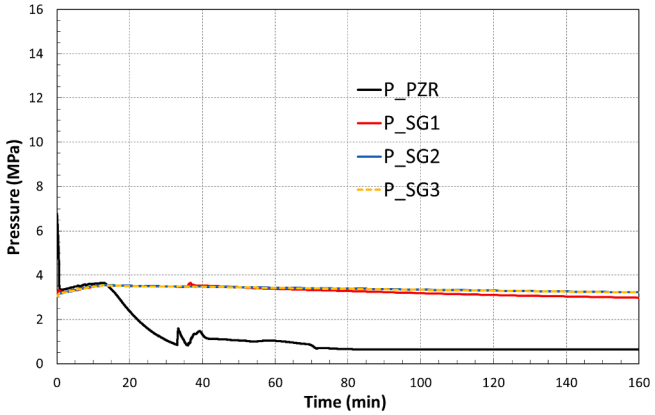

Fig. 5.1. Primary and secondary pressure (DEC-A).

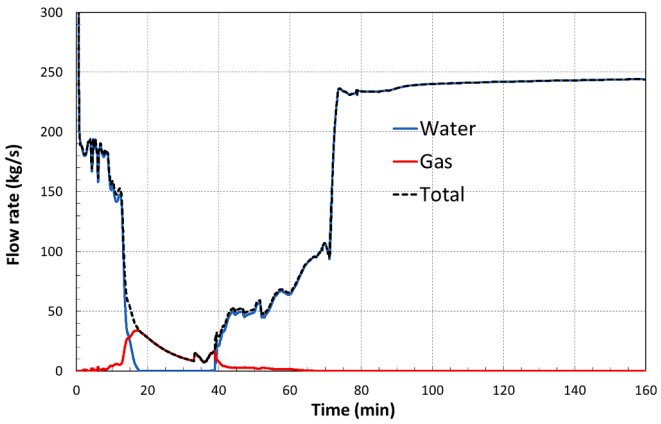

Fig. 5.2. Break mass flow rate (DEC-A).

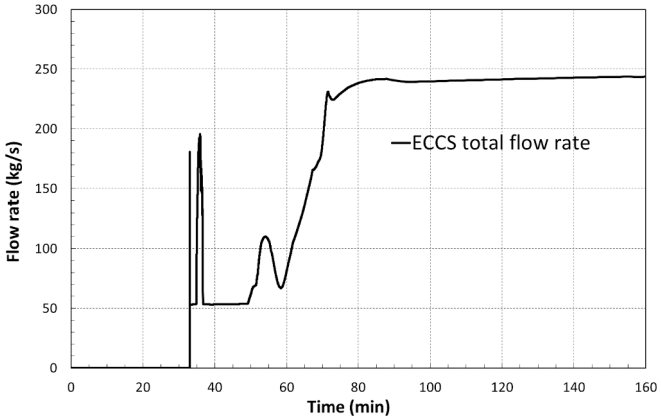

Fig. 5.3. Mass flow rate from the ECCS (DEC-A).

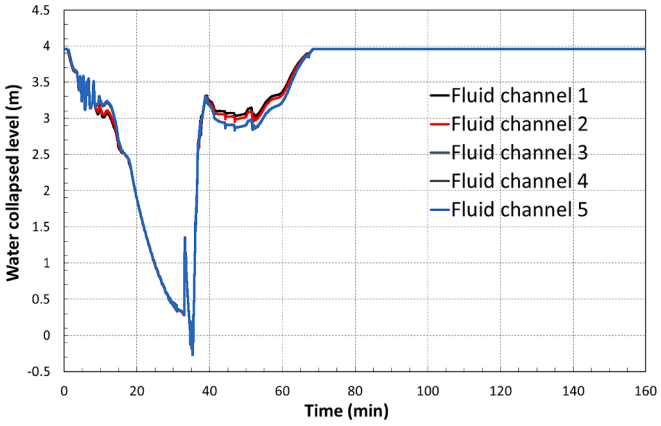

Fig. 5.4. Collapsed water level in the core (5 fluid channels) from BAF (DEC-A).

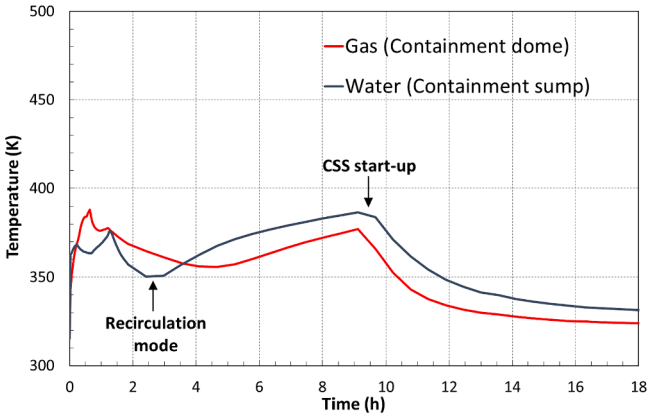

Fig. 5.5. Containment temperature (DEC-A).

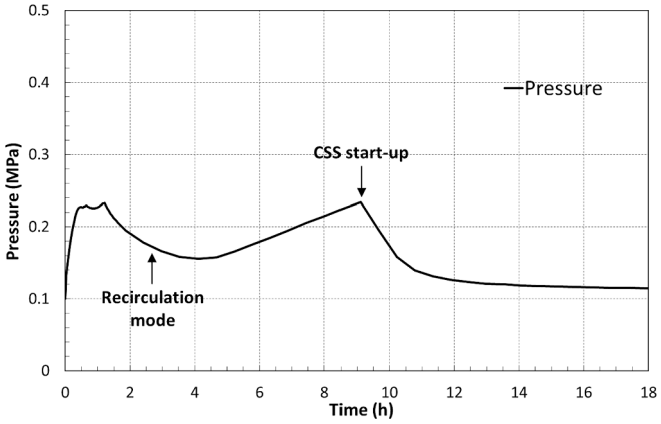

Fig. 5.6. Containment pressure (DEC-A).

(4″) is smaller than in the DBA scenario (16.3″), the pressure and temperature increase in the containment are slower.

In the long-term phase, the reestablishment of water mass inventory in the reactor primary system is more efficient than in DBA, due to the smaller size of the break, the complete availability of safety injection systems and lower decay-heat. At the end of simulated transient (48 h), the water collapsed level in the SGs primary side is above the water box and it stands in the U-tubes roughly involving the 2.5 % of their height. The reactor vessel is also filled by water, except the upper head (Fig. 3.1) where the void fraction is about 43 %. Regarding the containment, its behaviour is characterized, as in DBA, by small variations of

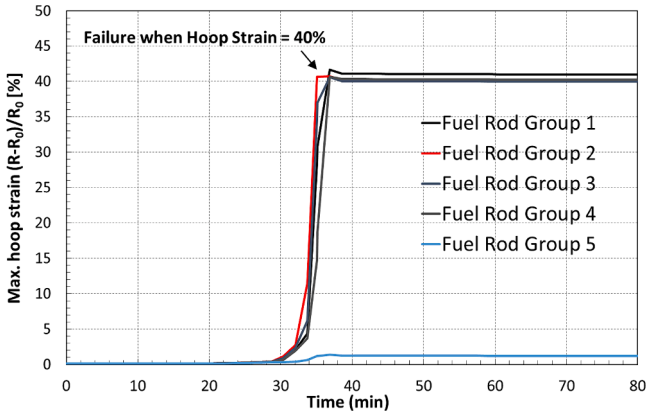

Fig. 5.8. Maximum clad hoop deformation in the 5 groups of fuel rods (DEC-A).

temperature and pressure. They increase again once the RWST is empty, and the recirculation mode starts. Then, with the CSS actuation (for a containment pressure > 2.4 bar), after approximately 9 h after the onset of accident, both the temperature and the pressure start to decrease.

Fig. 5.7 shows the Peak Cladding Temperature (PCT) evolution of both Case 1 (left) and Case 2 (right), for the 5 groups of fuel rods. One can observe that, due to the delayed activation of ECCS, the computed maximum cladding temperatures are higher in Case 2 than in Case 1, particularly the 2nd group of fuel rods. In this group, characterized by the maximum decay heat, a strong temperature escalation driven by Zr oxidation runaway was occurring leading to a very high temperature (2524 K), that is just below the UO_2 and ZrO_2 assumed solidus temperature (2550 K). Although the fuel melting temperature is not reached, a small local liquefaction of UO_2 by liquid Zr is observed putting this case at the boundary between DEC-A and DEC-B categories.

Minor differences of the timing of ECCS activation, can therefore lead to exceed or not the temperature at which the Zr oxidation kinetics is expected to be fast and temperature escalation is feared (1473 K).

During the transient, due both to the fuel rod heat-up and their internal pressure increase, claddings deform plastically. The calculated maximum hoop deformations in the different group of fuel rods, are displayed in Fig. 5.8 below. A slightly higher deformation rate is observed in the hottest fuel rod group (i.e. the 2nd one) but the differences between the different fuel rod groups (except for the 5th fuel rods group inside the peripheral channel) are small. The claddings in the four first fuel rod groups indeed deform very quickly near the top of the fissile column since the core uncovery and despite the ECCS actuation. The maximal increases in cladding diameters compared to their initial diameters is about 40 % in all these four fuel rod groups, limited then, by

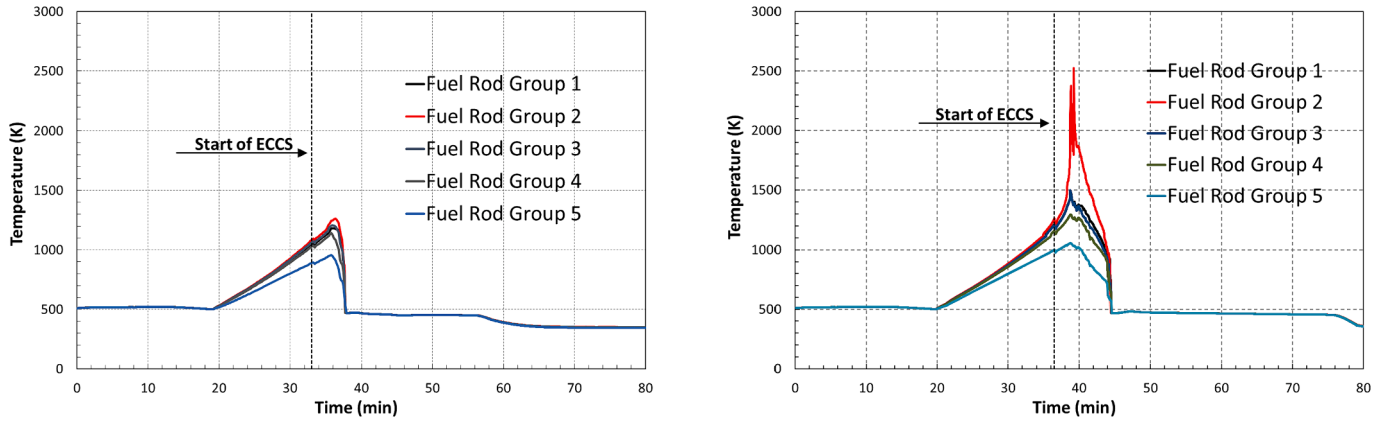

Fig. 5.7. Maximum cladding temperature in the 5 groups of fuel rods (DEC-A): Case 1 (left) and Case 2 (right) calculations.

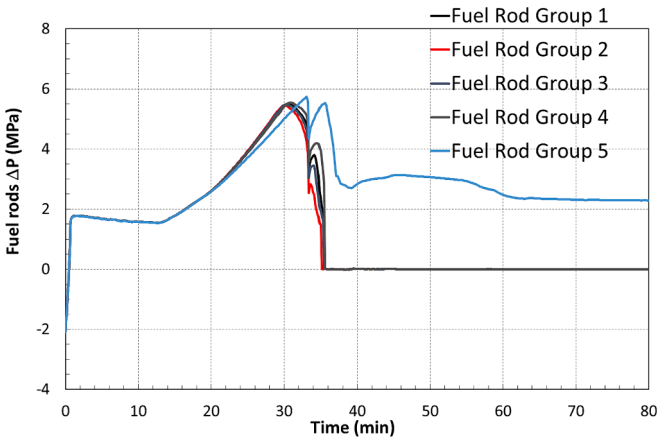

Fig. 5.9. Difference between the fuel rods internal pressure and the surrounding coolant in the 5 groups of fuel rods (DEC-A).

the assumed maximum allowed cladding hoop strain which immediately triggers the fuel rod failures even if the EDGAR burst criterion is not fulfilled.

The mentioned fuel rod failures are also proved by the evolution of the difference between the fuel rods internal pressure and the pressure of surrounding coolant during the transient, in the 5 groups of fuel rods, displayed in Fig. 5.9. After approximately 35 min from the accident start, the pressure difference in the first four fuel rods suddenly drops to 0, indicating the cladding failure. No clad failure is predicted in the peripheral fuel rod group characterized by a pressure difference which remains above 20 bar after core quenching.

The main data which characterize the cladding failures are provided by Table 5.1 below.

The total number of failed rods is 27,720 in both cases, corresponding to the first four fuel rods groups and accounting for 66.9 % of the total number of fuel rods in the core. As discussed before, the cladding failure of the four groups of rods occurred, for both Case 1 and Case 2, when the maximum cladding hoop deformation criterion of 40 % is reached.

No relevant differences are observed, between the two cases, on timing and elevation of cladding failures.

5.2. FPs behaviour from fuel to environment releases

The release of FPs from the core into the primary circuit is presented in Fig. 5.10. The release of volatile and semi-volatile elements contained in the fuel-cladding gap (Xe, Kr, I, Cs, Te, Ba and Sr), occurs stepwise at four instants, corresponding to the failure of four different fuel rod groups, as described above. Case 2 simulation is moreover characterized by a later release of other FPs, specifically semi or low-volatiles elements such as Mo, Ce, Ru, La, Y and Nb, as well as by an increase in the release of previously mentioned FPs. Such releases are observed after about 39 min from the initiating event and are justified by the high fuel temperature computed in the 2nd group of fuel rods, as well as by the onset of UO_2 liquefaction by liquid Zr, leading to release a fraction of FPs from fuel pellets, in addition to the gap inventory of failed fuel rods. Between the elements initially contained in the gap, the additional release from fuel is particularly noticeable, in comparison with gap release, for Te and, in a less extent, Ba (Fig. 5.10, right). In Case 1 simulation, the release of all FPs is almost entirely sustained by the gap inventory of failed fuel rods, the release from fuel pellets being absent or negligible.

Releases from the core to the RCS of some selected elements are summarized in Table 5.2 which also reports the retention in the RCS and the releases to the containment. In agreement with the discussion above, the release of FPs from the core to the RCS is in general higher in Case 2

Table 5.1
Characterization of cladding failures (DEC-A).

	Number of failed fuel rods		Failure time and (elevation from BAF)		Burst criterion triggering claddings failure	
	Case 1	Case2	Case 1	Case2	Case 1	Case2
Fuel rods 1	2376	2376	35.6 min (~3 m)	35.3 min (~3 m)	Max. hoop strain = 40 %	Max. hoop strain = 40 %
Fuel rods 2	5280	5280	35.1 min (~3 m)	34.9 min (~3 m)	Max. hoop strain = 40 %	Max. hoop strain = 40 %
Fuel rods 3	8448	8448	35.4 min (~3 m)	35.4 min (~3 m)	Max. hoop strain = 40 %	Max. hoop strain = 40 %
Fuel rods 4	11,616	11,616	35.6 min (~3 m)	36.0 min (~3 m)	Max. hoop strain = 40 %	Max. hoop strain = 40 %
Fuel rods 5	–	–	–	–	–	–
Total (fraction)	27,720 (66.9 %)	27,720 (66.9 %)				

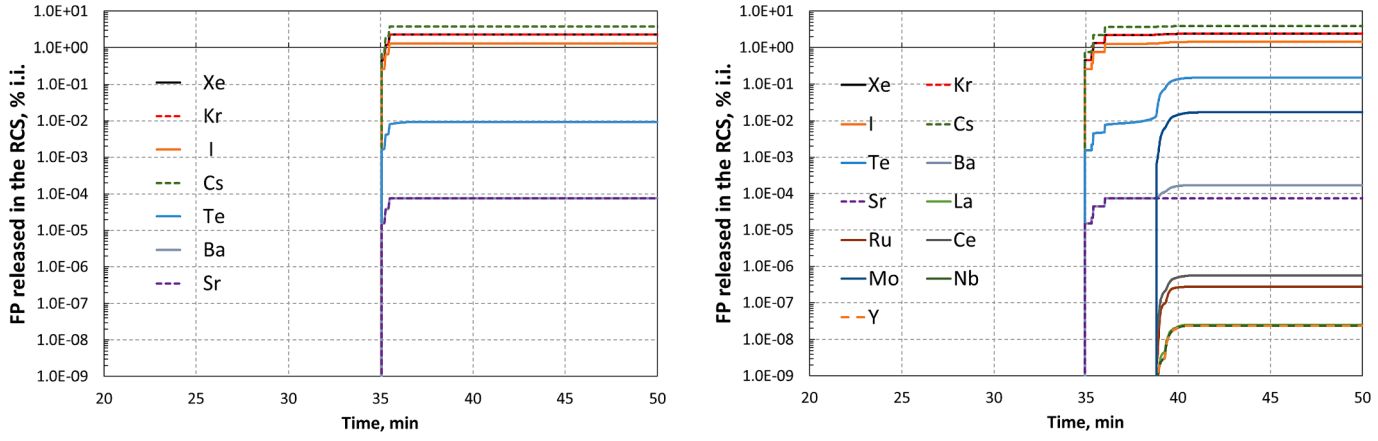

Fig. 5.10. FPs release from the core to the primary circuit in DEC-A scenario: Case 1 (left) and Case 2 (right) calculations.

Table 5.2
FPs release to the primary circuit and the containment building for the DEC-A scenario (48 h after the accident onset).

Element	Release to the RCS (% i.i.)		Retention in RCS (% of released FPs)		Release to the containment (% i.i.)	
	Case 1	Case 2	Case 1	Case 2	Case 1	Case 2
Xe	2.3E+00	2.4E+00	5.7E+00	4.1E+00	2.1E+00	2.3E+00
Kr	2.3E+00	2.4E+00	5.7E+00	4.1E+00	2.1E+00	2.3E+00
I	1.3E+00	1.4E+00	1.2E+01	1.1E+01	1.1E+00	1.3E+00
Cs	3.8E+00	3.9E+00	1.2E+01	6.0E+00	3.4E+00	3.6E+00
Te	9.4E-03	1.5E-01	1.9E+01	6.8E+01	7.6E-03	4.8E-02
Ba	7. 6E-05	1.7E-04	1.1E+01	4.3E+01	6.7E-05	9.7E-05
La	0.0E+00	2.5E-08	0.0E+00	7.1E+01	0.0E+00	7.2E-09
Ru	0.0E+00	2.7E-07	0.0E+00	7.5E+01	0.0E+00	7.0E-08
Sr	7.6E-05	7.4E-05	1.1E+01	3.3E+00	6.7E-05	7.2E-05
Ce	0.0E+00	5.6E-07	0.0E+00	7.3E+01	0.0E+00	1.5E-07
Mo	0.0E+00	1.7E-02	0.0E+00	7.4E+01	0.0E+00	4.5E-03
Nb	0.0E+00	2.4E-08	0.0E+00	7.0E+01	0.0E+00	7.0E-09
Y	0.0E+00	2.4E-08	0.0E+00	7.0E+01	0.0E+00	7.0E-09

than in Case 1. Significant differences are remarked for Te and Ba, whereas the differences on release of Xe, Kr, I and Cs are very small, since the additional release from fuel of such elements is not very significant in comparison with gap release. Release of strontium is however against the general trend, being its release to the RCS slightly lower in Case 2. It must be stressed that the release of such element derives almost completely from the gap inventory of the 4 ruptured fuel rod groups (according to Case 2 results, the Sr released by the fuel is about the 0.034 % of the gap release whereas the additional fuel release is completely absent in Case 2 simulation). Such gap inventory is slightly higher in Case 1 (due to the differences on radial distribution of FPs and decay heat showed in Table 2.1), providing an element of explanation for observed result. The semi or low-volatiles elements, which late release observed in Case 2 is triggered by high fuel temperature and UO_2 dissolution by liquid Zr, are of course not released at all in Case 1 simulation, characterized by much lower fuel temperatures.

The FPs retention in the primary circuit is generally lower in DEC-A than in DBA scenario, that is consistent with the shorter path from the core to the break (hot leg against cold leg in DBA).

However, according to Case 2 results, the elements characterized by a late release (Mo, Ce, Ru, La, Y and Nb) or by a significant increase of release (Te and Ba), at about 39 min (Fig. 5.10, right), exhibit a very high retention in the primary system, compared with results of Case 1 but also with the retention of other elements (Cs, I, Sr) whose additional release from fuel, in comparison with the gap release, is low or completely negligible, as in the case of Sr.

The retention behaviour observed in Case 2, not expected a priori, seems to be mainly determined by the sequence of events illustrated below.

After the cladding failures, the released FPs are transported in the gas phase from the core to the upper plenum and then into the broken hot leg, that is the shortest possible path to reach the break. When the ECCS is activated (36.5 min), the condensation induced by the water injection draws a flow of gas (steam and H_2), coming in a first time from the downcomer, that enter in the cold legs though the annular collector. During this phase, the steam produced in the core, as well as the eventually transported FPs, continue to get almost exclusively through the broken hot leg. At approximately 39 min, concurrently with the start of late or additional FPs release from fuel, the downcomer becomes full of water and, therefore, the condensation in the cold legs begins to draw a fraction of steam produced in the core that before was almost entirely flowing into the broken hot leg. Such branch of gas flow rate, transporting a part of FPs released from the core, enters the cold legs after having crossed the upper head and annular collector, thereby contributing to increase the retention in the primary system. Furthermore, the bottom part of the loop seal is shortly afterward obstructed by water, resulting in the formation of a gas (steam and H_2) pocket where a small amount of noble gases mass remains trapped and, with the progressive water recovery in the vessel, moves to the annular collector and upper head where remains until the end of simulated transient (Table 5.2). It is interesting to remark that the Sr (basically entirely released by the gap of failed fuel rods, being the additional release from fuel completely negligeable) shows the lowest retention in the primary system. Indeed, the instantaneous gap releases occur before the establishment of the additional flow path toward the cold legs, giving a rationale for the obtained result.

The hydraulic behaviour of Case 1 is similar to what observed in Case 2. However, as discussed before, the computed retention strongly depends on the simultaneousness between the FPs releases and the establishment of the additional flow path from the core to the cold legs (through upper head and annular collector). It is thought that the discrepancies observed in Table 5.2 between the two cases are at least in part determined by the different history of FPs release and activation time of the ECCS. One can see that the retention in the cold legs is slightly higher in Case 1 that in Case 2 for all elements except Te, Ba and of course the elements (Mo, Ce…) which release is not predicted by Case 1. The observed discrepancy is not negligible for the Sr that, as above discussed, is characterized by a very low retention in Case 2. In the Case 1 too, a small amount of noble gases mass remains in the vessel upper head (Table 5.2).

Moreover, we cannot fail to mention that the higher fuel temperature of Case 2, leading to higher gas temperature in the vessel and primary loops, can affect, in a selective way depending on considered element, the mechanisms of FPs deposition in the walls (e.g. partial re-evaporation of condensed Cs in the walls, mainly in CsOH chemical form, is observed during the high temperature phase of Case 2,) providing a further contribution to the observed discrepancies.

The FPs release to the containment building is the result of core

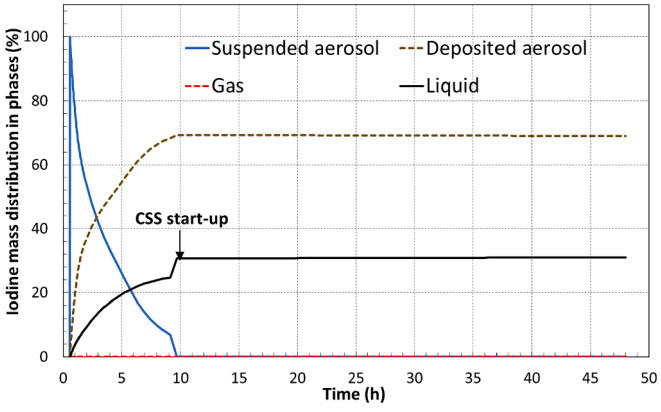

Fig. 5.11. Iodine mass distribution between different phases in the containment for DEC-A scenario.

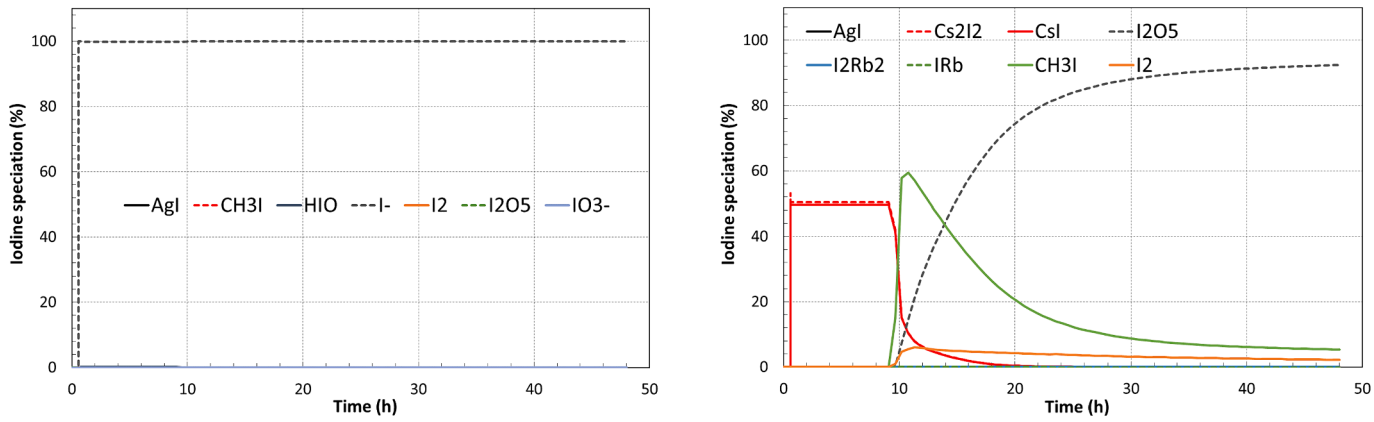

Fig. 5.12. Iodine speciation in the sumps (left) and the atmosphere (gaseous and suspended aerosols species) (right) in the containment for the DEC-A scenario.

Table 5.3
Cumulated activity (Bq) released in the environment, all leakage paths, by various isotopes after 48 h (DEC-A scenario).

Isotope	Radioactive period	Release to the environment (Bq)	
		Case 1	Case 2
Xe133	5.2 days	6.1E+13	6.0E+13
Xe133m	2.2 days	1.7E+12	1.6E+12
Xe135	9.1 h	2.0E+13	1.2E+13
Xe135m	15.6 min	1.8E+12	9.1E+11
Kr85M	4.5 h	1.6E+12	7.6E+11
Kr88	2.8 h	2.2E+12	8.4E+11
I131	8 days	2.8E+12	2.0E+12
I132	2.2 h	2.2E+12	7.0E+11
I133	21 h	4.9E+12	2.9E+12
I135	6.6 h	3.2E+12	1.3E+12
Cs134	2.1 years	1.1E+12	9.1E+11
Cs136	13 days	4.3E+11	3.0E+11
Cs137	30 years	7.8E+11	6.3E+11
Te131M	30 h	3.1E+09	8.7E+09
Te132	3.2 days	2.5E+10	9.9E+10
Ba137M	2.5 min	7.1E+11	5.9E+11
Ba140	12.7 days	2.8E+08	2.7E+08
Sr89	50.6 days	1.3E+08	1.1E+08
Sr90	28.9 years	9.2E+06	8.8E+06
Sr91	9.6 h	1.2E+08	6.3E+07
La140	1.6 days	0.0E+00	4.7E+07
Ru103	39.2 days	0.0E+00	1.8E+05
Ru106	372.6 days	0.0E+00	5.8E+04
Ce141	32.5 days	0.0E+00	4.2E+05
Ce144	285 days	0.0E+00	3.0E+05
Mo99	2.7 days	0.0E+00	1.2E+10
Nb95	35 days	0.0E+00	1.9E+04
Y90	2.6 days	0.0E+00	1.0E+06

release and retention in the RCS. All elements show, to a greater or lower degree depending on considered element, a higher release in the Case 2 than in the Case 1.

Fig. 5.11 presents the iodine distribution between different phases in the containment. Initially, iodine is present as suspended aerosols, which corresponds to initial release from the RCS to the containment. Quite rapidly after that, iodine aerosols are deposited on the walls of the containment by different mechanisms (diffusiophoresis, thermophoresis) or pass into the liquid phase (by gravitational settling). After 9 h since the start of the accident, the mass of iodine in suspended aerosol phase decreases sharply whereas the mass in the liquid phase increases. This behaviour is related to the start of the CSS, which accelerates the settling of aerosols towards the liquid phase. However, compared to the DBA scenario, by the end of the calculation, more iodine is found in the deposited aerosol form than the liquid form. This again can be explained by the operation of the CSS. In the DBA scenario, the CSS starts shortly after the initiating event, before the release of FPs. When these arrive in the containment, the gravitational settling, promoted by the CSS droplets, are the dominant aerosol deposition mechanism. In the DEC-A scenario, at the moment of FPs release to the containment, the CSS is not yet in service, so other aerosol deposition phenomena, such as thermophoresis and diffusiophoresis, are dominant over gravitational settling. The gaseous fraction of iodine in the containment remains low as in DBA scenario.

Regarding the iodine speciation in the liquid phase of the containment, the results aren't different from the DBA scenario. The most abundant species is the iodide ion I^- (Fig. 5.12 left), which is formed from the dissociation of metallic iodide aerosols (CsI, Cs_2I_2) in the sumps. The major forms of iodine species in the containment atmosphere are the CsI and the Cs_2I_2 aerosols, particularly in the initial stage of the accident. Then, after the start of the CSS and the settling of aerosols, the major species for a short period of time becomes the gaseous organic iodine CH3I. In the later stages of the accident, as in the DBA transient, the dominant form are the iodine oxide aerosols (I_2O_5) with a small amount of organic iodine, which are formed from gaseous species under the effect of radiation. Despite this, the absolute value of the quantity of iodine in suspended aerosol or gaseous form in the containment is insignificant, since most aerosols have settled on the walls or in the sump during the first 10 h after the start of the accident (see Fig. 5.11).

Table 5.3 presents the released activity in the environment for several isotopes of interest for RC evaluation 48 h after the initiating event. Xenon and iodine isotopes contribute the most to the released activity, followed by krypton and caesium. Despite presenting a lower release fraction to the containment building for all the FPs of Table 5.2, the activity released into the environment is generally higher in Case 1 than it is in Case 2 calculation because of the hypotheses regarding the leaks of the containment building (direct release from containment to environment in Case 1).

Table 5.4
Computed dose (adults) at 1 km from emission point 2 days from accident onset (DEC-A).

	Thyroid equivalent dose (mSv)	Effective dose (mSv)		
		External exposition	Inhalation	Total
Case 1	1.7938	0.0107	0.2540	0.2643
Case 2	0.6642	0.0035	0.0995	0.1030

The very high fuel temperature, reached in the Case 2 simulation, plays a key role only for isotopes of elements characterized by late (La, Ru…) or very significant additional release from fuel pellets, as the case of tellurium. Such radionuclides exhibit higher activity release in the environment in Case 2 than in Case 1 simulation. In the case of barium isotopes, the additional release observed in Case 2, being much lower than the one of tellurium, is not enough to prevail against the conservative hypotheses concerning the leaks of the containment and the activities of Ba137m and Ba140 are once again higher in Case 1 than in Case 2.

As for DBA, Table 5.4 reports, for adults, the thyroid equivalent dose and the total effective dose, by distinguishing external exposition and inhalation, at 1 km from emission point, 2 days from the accident onset.

As expected, and mainly due to the higher number of failed fuel rods and higher fuel temperature, the estimated dose is higher than in the DBA case remaining however limited enough. Again, in agreement with cumulated activity released to the environment, the computed dose is higher in Case 1 than in Case 2.

6. Conclusions

The DBA and DEC-A LOCA scenarios, simulated with ASTEC in a PWR 900 MWe as well as the sensitivity studies performed, allowed to draw the following observations on the present code capability and to highlight the need of further improvements of code models and calculation schemes.

ASTEC code demonstrated to be a valuable tool to characterize, in a single computation, the thermal behaviour of the core, the number of failed rods and the release of FPs into the environment, this latter required for the estimation of RC of the analysed transients. The ASTEC calculation scheme considers a radial discretization of reactor core distinguishing five groups of fuel rods contained into five radial fluid channels. Such radial nodalization is normally used for SA analysis but it could be not detailed enough to accurately estimate the number of failed rods and ST in case of DBA and DEC-A scenarios.

Performed simulation outlined that, user choices on cladding burst criterion can have a not negligible effect on the predicted number of failed rods and resulting FPs release. CHAPMAN burst criterion (burst temperature function of engineering stress and temperature derivative) proved to be more conservative that EDGAR one and sensitivity calculations of DBA scenario, demonstrated that the cladding failure can be predicted by EDGAR criterion (true burst stress vs. cladding temperature) only in case of the most pessimistic conditions (i.e. combining an increase of the fuel rod internal pressure and considering a pronounced peak factor on axial and radial power distribution).

A reassessment of these DBA and DEC-A scenarios is in progress, within the task 2.5 of R2CA that contemplates a second run of reactor calculations, by using improved models and calculation chains which are mainly focussed on a new core modelling and updated fuel clad failure models with the objective to better estimate the number of failed rods.

A new core model, characterized by a higher number of representative rods inside each radial fluid channel, will be adopted in ASTEC code simulations. A more challenging option is to use the DRACCAR code (Glantz et al., 2018) and in particular the ICARE3D module for the core simulation. For this purpose, an innovative approach to describe the whole reactor core with a level of details allowing an accurate estimation of failed rods, is studied within the R2CA project.

Moreover, new criteria for clad failure, based on the re-assessment of the available experimental database gathering more than 1400 tests, have been established and will be tested.

Beyond what is made within the task 2.5 of the project, it is important to point out that the ASTEC features and models, briefly illustrated hereafter, must be taken into account to further improve the reliability of the code on the simulation of DBA and DEC-A LOCA transients.

The distribution of FPs and the decay heat in the core can be provided by users through a limited number of parameters that doesn't allow for an accurate enough representation of real reactor conditions. The possibility to provide independent FPs inventory for each group of fuel rods, also distinguishing between fuel pellets and gap, would be an important improvement of the code. It is worth noting that the gap inventory is the main source of FPs release in transients characterized by relatively low fuel temperatures and thus, an accurate characterization of such parameter at the start of the accident is a crucial point for a suitable estimation of total FPs release.

Another point is that the 1D (z) clad deformation model assuming a circular shape is not adapted to predict potential contact between neighbouring fuel rods and the corresponding average clad diameter, calculated according to the creep deformation, can exceed the rod pitch. The maximum hoop strain assuming a circular shape is limited by a user's parameter which default value has been set to 40 % in order to prevent for large and unrealistic overlapping between adjacent fuel rods. Such user parameter also triggers the cladding failure and, as discussed in the paper, it is often fulfilled before reaching the selected main burst criterion. In such cases, the prediction of cladding burst is entrusted exclusively by the maximum hoop strain set by user's that is clearly inadequate for code applications oriented to the estimation of the number of failed rods. To address the outlined limitation, the user parameter setting the maximum allowed hoop strain should be replaced by a more comprehensive model able to manage the non-axisymmetric cladding ballooning and the contact between neighbouring fuel rods. A specific and simplified method to address this topic in ASTEC and the corresponding algorithm has been proposed within the project and should be implemented in the code in the future.

7. Disclaimer

Views and opinions expressed in this paper reflect only the author's view and the European Commission is not responsible for any use that may be made of the information it contains.

CRediT authorship contribution statement

Stefano Ederli: Conceptualization, Software, Formal analysis, Data curation, Writing – original draft. **Patrick Drai:** Conceptualization, Software, Formal analysis, Data curation, Writing – original draft. **Dorel Obada:** Conceptualization, Software, Formal analysis, Data curation, Writing – original draft. **Nathalie Girault:** Conceptualization, Software, Formal analysis, Methodology, Project administration, Funding acquisition, Supervision, Resources, Writing – original draft, Validation. **Fulvio Mascari:** Conceptualization, Resources, Formal analysis, Writing – original draft, Validation.

Declaration of competing interest

The authors declare that they have no known competing financial interests or personal relationships that could have appeared to influence the work reported in this paper.

Data availability

Data will be made available on request.

Acknowledgement

Funding: This project has received funding from the Euratom research and training programme 2014-2018 under grant agreement No 847656.

References

Bradt, P. Review of the radiological consequences evaluation methodologies, R2CA internal report, March 2021.

Chailan, L., et al, Overview of the ASTEC code and models for evaluation of Severe Accidents in Water Cooled Reactors, IAEA Technical meeting on the Status and evaluation of Severe Accidents simulation codes for Water Cooled Reactors, Vienna (Austria), October 2017, 9-12.

Chapman, R.H., 1979. "Multi-rod burst test", program Progress report april-june 1979 USNRC report – ORNL/NUREG/CR-1023. Oak Ridge National Laboratory, TN (USA).

Chatelard, P., et al., July 2016. Main modelling features of ASTEC v2.1 major version. Ann. Nucl. Energy vol. 93, 83–93. https://doi.org/10.1016/j.anucene.2015.12.026.

Chatelard, P., et al., 2017. D40.45 – set of final" reference" NPP ASTEC input decks. Report of EU-CESAM Project.

Coindreau, O., 2020. ASTEC V2.2: physical modelling of the ICARE module. IRSN Report IRSN/2016-00422, Cadarache.

Defence in depth in nuclear safety – INSAG 10 – IAEA – VIENNA – 1996.

EU 19841 Determination of the in-containment source term for a Large-Break Loss of Coolant Accident, Final report, Contract B4-3070-97-810-MBL-C2; EUR 19841 EN, European Commission, Brussels (Belgium), April 2001.

Glantz, T., Taurines, T., de Luze, O., Belon, S., Guillard, G., et al., 2018. DRACCAR a multi-physics code for computational analysis of multi-rod ballooning and fuel relocation during LOCA transients Part one general modeling description. Nuclear Engineering and Design, Elsevier 339, 269–285. https://doi.org/10.1016/j.nucengdes.2018.06.022 https://hal.science/hal-02881798.

International Atomic Energy Agency, "Safety of Nuclear Power Plants: Design", IAEA Safety Standards Series No. SSR-2/1 (Rev. 1), IAEA, VIENNA, 2016.

International Atomic Energy Agency, "Current Approaches to the Analysis of Design Extension Conditions WITH Core Melting for New Nuclear Power Plants", IAEA-TECDOC-1982, IAEA, Vienna, 2021.

International Nuclear and Radiological Event Scale (INES), accessed 5 May 2023, accessed 5 May 2023, "https://www.iaea.org/resources/databases/international-nuclear-and-radiological-event-scale".

Level 2 Probabilistic Safety Assessment for French PWR 900 MWe – IRSN technical report - Confidential, Fontenay aux Roses, 2008.

Nowack, H., Chatelard, P., Chailan, L., Hermsmeyer, St., Sanchez, V., Herranz, L. CESAM – Code for European Severe Accident Management, EURATOM Project on ASTEC Improvement, Annals of Nuclear Energy, Vol. 116, June 2018, Pages 128–136.

Pettersson, K., et al., 2009. "Nuclear fuel behaviour in loss-of-coolant accident (LOCA) conditions. OECD-NEA, Paris, France, p. 369. State-of-the-art-report", in.

Powers, D.A., Meyer, R.O. Cladding swelling and rupture models for LOCA analysis, Technical Report NUREG-630, Washington D.C., 1980.

Raimond, E., et al., 2013. ASAMPSA2 best-practices guidelines for L2PSA development and applications. Technical Report ASAMPSA2/WP2-3-4/D3.3D2013-35, ASAMPSA2 Project.

Regulatory Guide 1.195, Methods and assumptions for evaluating radiological consequences of design basis accidents at light-water nuclear power plants. U.S. Nuclear Regulatory Commission, Washington D.C., May 2003.

OECD-FFRD Report on Fuel Fragmentation, Relocation and Dispersal, NEA/CSNI/R (2016)16, 201, Paris (France), October 2016.

Ritzman, R.L., et al., "Release of radioactivity in reactor accidents. Appendix VII to Reactor Safety Studies", WASH-1400, NUREG 75/014, US NRC, Washington D.C., October 1975.

Taurines, T., Glantz, T., Belon, S. (IRSN), Kulacsy, K. (EK), Király, K. (EK), Nagy, R. (EK), Szabó, P. (VTT), Dif, B. (VTT), Arkoma, A. (VTT). New Burst Criteria for Loss Of Coolant Accidents Radiological Consequences Assessment, Annals of Nuclear Energy, To be published in this issue.

Taurines, T., Belon, S. (IRSN), Arkoma, A. (VTT), Kaliatka, T. (LEI), Kulacsy, K. (EK), Jobst, M. (HZDR), Ovdiienko, I. (SSTC), Van Uffelen, P. (JRC), Klouzal, J. (UJV), Calabrese, R, (ENEA). "Rod cladding failure during LOCA- Final report on experimental database reassessment and model/code improvements", Deliverable D3.4 of R2CA project, 2023.

The ASTEC Software Package, accessed 5 June 2023 "https://en.irsn.fr/EN/Research/Scientific-tools/Computer-codes/Pages/The-ASTEC-Software-Package-2949.aspx".

Topin, V., Carenini, L., Coindreau, O., Laborde, L., 2021. ASTEC ICARE module user manual. IRSN Report IRSN/2021-00300, Caradache.

WENRA Safety Reference Level for Existing Reactors – February 2021.